A&A 557, A85 (2013)
DOI: 10.1051/0004-6361/201219165

Astronomy & Astrophysics

Binary black holes in nuclei of extragalactic radio sources

J. Roland[1], S. Britzen[2], A. Caproni[3], C. Fromm[2], C. Glück[4], and A. Zensus[2]

[1] Institut d'Astrophysique, UPMC Univ. Paris 06, CNRS, UMR 7095, 98bis Bd Arago, 75014 Paris, France
e-mail: roland@iap.fr
[2] Max-Planck-Institut für Radioastronomie, Auf dem Hügel 69, 53121 Bonn, Germany
[3] Núcleo de Astrofísica Teórica, Universidade Cruzeiro do Sul, R. Galvão Bueno 868, Liberdade, 01506-000 São Paulo, SP, Brazil
[4] I. Physikalisches Institut, Universität zu Köln, Zülpicher Str. 77, 50937 Köln, Germany

Received 5 March 2012 / Accepted 5 June 2013

ABSTRACT

If we assume that nuclei of extragalactic radio sources contain binary black hole systems, the two black holes can eject VLBI components, in which case two families of different VLBI trajectories will be observed. Another important consequence of a binary black hole system is that the VLBI core is associated with one black hole, and if a VLBI component is ejected by the second black hole, one expects to be able to detect the offset of the origin of the VLBI component ejected by the black hole that is not associated with the VLBI core. The ejection of VLBI components is perturbed by the precession of the accretion disk and the motion of the black holes around the center of gravity of the binary black hole system. We modeled the ejection of the component taking into account the two pertubations and present a method to fit the coordinates of a VLBI component and to deduce the characteristics of the binary black hole system. Specifically, this is the ratio T_p/T_b where T_p is the precession period of the accretion disk and T_b is the orbital period of the binary black hole system, the mass ratio M_1/M_2, and the radius of the binary black hole system R_{bin}. From the variations of the coordinates as a function of time of the ejected VLBI component, we estimated the inclination angle i_o and the bulk Lorentz factor γ of the modeled component. We applied the method to component S1 of 1823+568 and to component C5 of 3C 279, which presents a large offset of the space origin from the VLBI core. We found that 1823+568 contains a binary black hole system whose size is $R_{bin} \approx 60$ μas (μas is a microarcsecond) and 3C 279 contains a binary black hole system whose size is $R_{bin} \approx 420$ μas. We calculated the separation of the two black holes and the coordinates of the second black hole from the VLBI core. This information will be important to link the radio reference-frame system obtained from VLBI observations and the optical reference-frame system obtained from *Gaia*.

Key words. astrometry – galaxies: jets – galaxies: individual: 1823+568 – galaxies: individual: 3C 279

1. Introduction

VLBI observations of compact radio sources show that the ejection of VLBI components does not follow a straight line, but undulates. These observations suggest a precession of the accretion disk. To explain the precession of the accretion disk, we assumed that the nuclei of radio sources contain binary black hole systems (BBH system, see Fig. 1).

A BBH system produces three pertubations of the VLBI ejection due to

1. the precession of the accretion disk;
2. the motion of the two black holes around the center of gravity of the BBH system; and
3. the motion of the BBH system in the galaxy.

In this article, we do not take into account the possible third pertubation due to the motion of the BBH system in the galaxy.

A BBH system induces several consequences, which are that

1. even if the angle between the accretion disk and the plane of rotation of the BBH system is zero, the ejection does not follow a straight line (due to the rotation of the black holes around the center of gravity of the BBH system);
2. the two black holes can have accretion disks with different angles with the plane of rotation of the BBH system and can eject VLBI components; in that case we observe two different families of trajectories; a good example of a source with two families of trajectories is 3C 273, whose components C5 and C9 follow two different types of trajectories (see Fig. 2); and
3. if the VLBI core is associated with one black hole, and if the VLBI component is ejected by the second black hole, there will be an offset between the VLBI core and the origin of the ejection of the VLBI component; this offset will correspond to the radius of the BBH system.

Fig. 1. BBH system model. The two black holes can have an accretion disk and can eject VLBI components. If it is the case, we observe two different families of trajectories and an offset between the VLBI core and the origin of the VLBI component if it is ejected by the black hole that is not associated with the VLBI core. The angles Ω_1 and Ω_2 between the accretion disks and the rotation plane of the BBH system can be different.

The precession of the accretion disk can be explained using a single rotating black hole (Lense-Thirring effect) or by the magnetically driven precession (Caproni et al. 2006). However, a single black hole and a BBH system have completely different consequences. In the case of a BBH system, one has an extra perturbation of the ejected component due to the motions of the black holes around the center of gravity of the BBH system. One can expect to observe two different families of trajectories (if the two

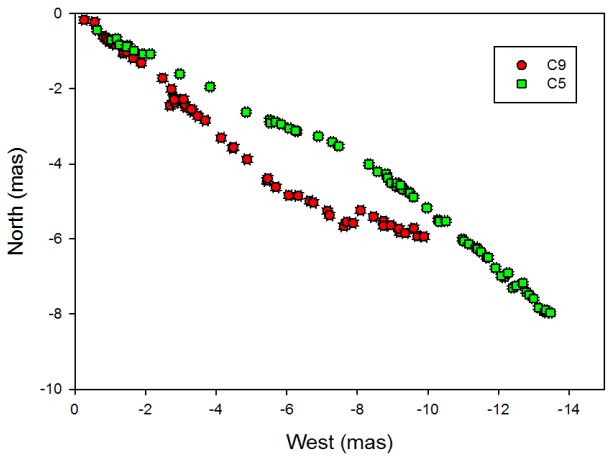

Fig. 2. Trajectories of the VLBI components C5 and C9 of 3C 273 using MOJAVE data (Lister et al. 2009b). We observe two different types of trajectories, suggesting that they are ejected from two different black holes.

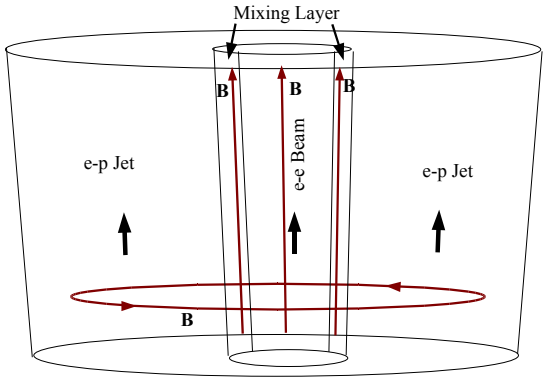

Fig. 3. Two-fluid model. The outflow consists of an $e^- - e^+$ plasma, *the beam*, moving at a highly relativistic speed, surrounded by an $e^- - p$ plasma, and of *the jet*, moving at a mildly relativistic speed. The magnetic field lines are parallel to the flow in the beam and the mixing layer, and are toroidal in the jet.

black holes eject VLBI components) and an offset of the origin of the ejected component if it is ejected by the black hole that is not associated with the VLBI core.

We modeled the ejection of the VLBI component using a geometrical model that takes into account the two main perturbations due to the BBH system, i.e.

1. the precession of the accretion disk; and
2. the motion of the two black holes around the center of gravity of the BBH system.

Modeling the ejection of VLBI components using a BBH system has been developed in previous articles, for instance Britzen et al. (2001) modeled 0420-014, Lobanov & Roland (2005) modeled 3C 345, and Roland et al. (2008) modeled 1803+784. Observationnal VLBI studies have been performed to directly detect BBH systems in active galactic nuclei (Burke-Spolaor 2011; Tingay & Wayth 2011).

In Sect. 2 we recall the main lines of the model. The details of the model can be found in Roland et al. (2008).

We determined the free parameters of the model by comparing the observed coordinates of the VLBI component with the calculated coordinates of the model.

This method requires knowing of the variations of the two coordinates of the VLBI component as a function of time. Because these observations contain the kinematical information, we will be able to estimate the inclination angle of the source and the bulk Lorentz factor of the ejected component.

In this article we present a method to solve this problem, either for a precession model or for a BBH system model, based on understanding the space of the solutions.

Practically, two different cases can occur when we try to solve this problem.

1. Either the VLBI component is ejected from the VLBI core, or the offset is smaller than or on the order of the smallest error bars of the VLBI positions of the ejected component (case I);
2. or the VLBI component is ejected with an offset larger than the smallest error bars of the VLBI positions of the ejected component (case II).

Case II is much more complicated to solve than case I, because the observed coordinates contain an unknown offset that is larger than the error bars. Therefore, we first have to find the offset, then correct the VLBI data from the offset, and finally find the solution corresponding to the corrected data.

We present the method for solving the problem in Sect. 3. To illustrate case I, we solve the fit of component S1 of 1823+568 using MOJAVE data in Sect. 4. To illustrate case II, we solve the fit of component C5 of 3C 279 using MOJAVE data in Sect. 5.

2. Model

2.1. Introduction: two-fluid model

We describe the ejection of a VLBI component in the framework of the two-fluid model (Sol et al. 1989; Pelletier & Roland 1989, 1990; Pelletier & Sol 1992). The two-fluid description of the outflow is adopted with the following assumptions:

1. The outflow consists of an $e^- - e^+$ plasma (hereafter *the beam*) moving at a highly relativistic speed (with corresponding Lorentz factor[1] $\gamma_b \leq 30$) surrounded by an $e^- - p$ plasma (hereafter *the jet*) moving at a mildly relativistic speed of $v_j \leq 0.4 \times c$.
2. The magnetic field lines are parallel to the flow in the beam and the mixing layer, and are toroidal in the jet (see Fig. 3).

Muxlow et al. (1988) and Roland et al. (1988) found that the Cygnus A hot spots could be explained by a an $e^- - p$ plasma moving at a mildly relativistic speed, i.e. $v_j \leq 0.4 \times c$. Consequently, the two-fluid model was introduced to explain superluminal radio sources observed in the nuclei of radio sources.

The $e^- - p$ jet carries most of the mass and the kinetic energy ejected by the nucleus. It is responsible for the formation of kpc-jets, hot spots, and extended lobes (Roland & Hetem 1996). The relativistic $e^\pm$ beam moves in a channel through the mildly relativistic jet and is responsible for the formation of superluminal sources and their γ-ray emission (Roland et al. 1994). The relativistic beam can propagate when the magnetic field B is parallel to the flow in the beam and in the mixing layer between the beam and the jet, and when it is greater than a critical value (Pelletier et al. 1988; Achatz & Schlickeiser 1993). The magnetic field in the jet becomes rapidly toroidal as a function of distance from the core (Pelletier & Roland 1990).

[1] The bulk Lorentz factor is limited to 30 to ensure the propagation stability of the relativistic beam in the subrelativistc jet.

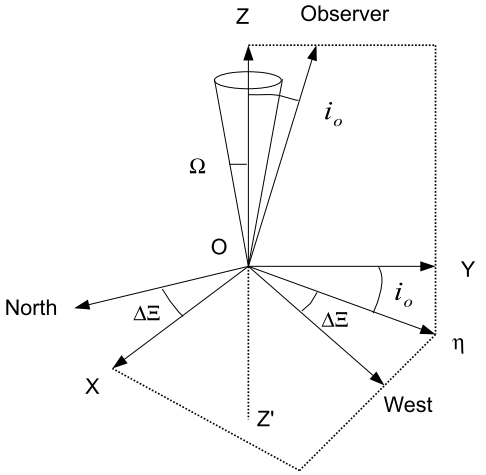

Fig. 4. Geometry of the problem. The planes X–η and west–north are perpendicular to the line of sight. In the west–north plane, the axis η corresponds to the mean ejection direction of the VLBI component. Ω is the opening angle of the precession cone.

The observational evidence for the two-fluid model has been discussed by e.g. Roland & Hetem (1996). Observational evidence for relativistic ejection of an $e^{\pm}$ beam comes from the γ-ray observations of MeV sources (Roland & Hermsen 1995; Skibo et al. 1997) and from VLBI polarization observations (Attridge et al. 1999).

The formation of X-ray and γ-ray spectra, assuming relativistic ejection of $e^{\pm}$ beams, has been investigated by Marcowith et al. (1995, 1998) for Centaurus A.

The possible existence of VLBI components with two different apparent speeds has been pointed out for the radio galaxies Centaurus A (Tingay et al. 1998), Virgo A (Biretta et al. 1999) and 3C 120 (Gómez et al. 2001). If the relativistic beam transfers some energy and/or relativistic particles to the jet, the relativistic particles in the jet will radiate and a new VLBI component with a mildly relativistic speed will be observed (3C 120 is a good example of a source showing this effect).

2.2. Geometry of the model

We call Ω the angle between the accretion disk and the orbital plane (XOY) of the BBH system. The component is ejected on a cone (the precession cone) with its axis in the $Z'OZ$ plane and of opening angle Ω. We assumed that the line of sight is in the plane (YOZ) and forms an angle i_o with the axis $Z'OZ$ (see Fig. 4). The axis η corresponds to the mean ejection direction of the VLBI component projected in a plane perpendicular to the line of sight, so the plane perpendicular to the line of sight is the plane (ηOX). We call ΔΞ the rotation angle in the plane perpendicular to the line of sight to transform the coordinates η and X into coordinates N (north) and W (west), which are directly comparable with the VLBI observations. We have

$$W = -x\cos(\Delta\Xi) + (z\sin(i_o) + y\cos(i_o))\sin(\Delta\Xi), \quad (1)$$

$$N = x\sin(\Delta\Xi) + (z\sin(i_o) + y\cos(i_o))\cos(\Delta\Xi). \quad (2)$$

The sign of the coordinate W was changed from Roland et al. (2008) to use the same definition as VLBI observations.

2.3. General perturbation of the VLBI ejection

For VLBI observations, the origin of the coordinates is black hole 1, i.e. the black hole ejecting the VLBI components. For the sake of simplicity, we assumed that the two black holes have circular orbits, i.e. e = 0. Therefore, the coordinates of the moving components in the frame of reference where black hole 1 is considered the origin are (Roland et al. 2008)

$$x_c = [R_o(z)\cos(\omega_p t - k_p z(t) + \phi_o) + x_1\cos(\omega_b t - k_b z(t) + \psi_o) - x_1\cos(\psi_o)]\exp(-t/T_d), \quad (3)$$

$$y_c = [R_o(z)\sin(\omega_p t - k_p z(t) + \phi_o) + y_1\sin(\omega_b t - k_b z(t) + \psi_o) - y_1\sin(\psi_o)]\exp(-t/T_d), \quad (4)$$

$$z_c = z_c(t), \quad (5)$$

where

- $R_o(z)$ is the amplitude of the precession perturbation, given by $R_o(z) = R_o z_c(t)/(a + z_c(t))$, with $a = R_o/(2\tan\Omega)$;
- ω_p is $\omega_p = 2\pi/T_p$, where T_p is the precession period, and k_p is defined by $k_p = 2\pi/T_p V_a$, where V_a is the speed of the propagation of the perturbations;
- ω_b is $\omega_b = 2\pi/T_b$, where T_b is the BBH system period and k_b is defined by $k_b = 2\pi/T_b V_a$;
- T_d is the characteristic time of the damping of the perturbation;
- x_1 and y_1 are given by

$$x_1 = y_1 = -\frac{M_2}{M_1 + M_2} \times \left[\frac{T_b^2}{4\pi^2} G(M_1 + M_2)\right]^{1/3}. \quad (6)$$

We define with R_{bin} the distance between the two black holes as the size of the BBH system. It is

$$R_{bin} = \left[\frac{T_b^2}{4\pi^2} G(M_1 + M_2)\right]^{1/3}. \quad (7)$$

In mas units (milli arc second units), it is

$$R_{bin} \approx 2.06 \times 10^8 \left[\frac{T_b^2}{4\pi^2} G(M_1 + M_2)\right]^{1/3} / D_a, \quad (8)$$

where $D_a = D_l/(1+z)^2$ is the angular distance, D_l is the luminosity distance, and z is the redshift of the source.

The differential equation governing the evolution of $z_c(t)$ can be obtained by defining the speed of the component, namely

$$v_c^2 = \left(\frac{dx_c(t)}{dt}\right)^2 + \left(\frac{dy_c(t)}{dt}\right)^2 + \left(\frac{dz_c(t)}{dt}\right)^2, \quad (9)$$

where v_c is related to the bulk Lorentz factor by $v_c/c = \sqrt{(1 - 1/\gamma_c^2)}$.

Using (3)–(5), we find from (9) that dz_c/dt is the solution of the equation

$$A\left(\frac{dz_c}{dt}\right)^2 + B\left(\frac{dz_c}{dt}\right) + C = 0. \quad (10)$$

The calculation of the coefficients A, B and C can be found in Appendix A of Roland et al. (2008).

Equation (10) admits two solutions corresponding to the jet and the counter-jet.

Following Camenzind & Krockenberger (1992), if we call θ the angle between the velocity of the component and the line of sight, we have

$$\cos(\theta(t)) = \left(\frac{dy_c}{dt}\sin i_o + \frac{dz_c}{dt}\cos i_o\right)/v_c. \quad (11)$$

The Doppler beaming factor δ, characterizing the anisotropic emission of the moving component, is

$$\delta_c(t) = \frac{1}{\gamma_c\,[1-\beta_c\cos(\theta(t))]}, \tag{12}$$

where $\beta_c = v_c/c$. The observed flux density is

$$S_c = \frac{1}{D_l^2}\delta_c(t)^{2+\alpha_r}(1+z)^{1-\alpha_r}\int_c j_c \mathrm{d}V, \tag{13}$$

where D_l is the luminosity distance of the source, z its redshift, j_c is the emissivity of the component, and α_r is the synchrotron spectral index (it is related to the flux density by $S \propto \nu^{-\alpha_r}$). As the component is moving relativistically toward the observer, the observed time is shortened and is given by

$$t_{obs} = \int_0^t [1-\beta_c\cos(\theta(t'))]\,(1+z)\,\mathrm{d}t'. \tag{14}$$

2.4. Coordinates of the VLBI component

Solving (10), we determine the coordinate $z_c(t)$ of a point-source component ejected relativistically in the perturbed beam. Then, using (3) and (4), we can find the coordinates $x_c(t)$ and $y_c(t)$ of the component. In addition, for each point of the trajectory, we can calculate the derivatives $\mathrm{d}x_c/\mathrm{d}t$, $\mathrm{d}y_c/\mathrm{d}t$, $\mathrm{d}z_c/\mathrm{d}t$ and then deduce $\cos\theta$ from (11), δ_c from (12), S_ν from (13) and t_{obs} from (14).

After calculating the coordinates $x_c(t)$, $y_c(t)$ and $z_c(t)$, they can be transformed to $w_c(t)$ (west) and $n_c(t)$ (north) coordinates using (1) and (2).

As explained in Britzen et al. (2001), Lobanov & Roland (2005), and Roland et al. (2008), the radio VLBI component has to be described as an extended component along the beam. We call n_{rad} the number of points (or integration steps along the beam) for which we integrate to model the component. The coordinates $W_c(t)$, $N_c(t)$ of the VLBI component are then

$$W_c(t) = \left(\sum_{i=1}^{n_{rad}} w_{ci}(t)\right)/n_{rad} \tag{15}$$

and

$$N_c(t) = \left(\sum_{i=1}^{n_{rad}} n_{ci}(t)\right)/n_{rad} \tag{16}$$

and can be compared with the observed coordinates of the VLBI component, which correpond to the radio peak intensity coordinates provided by model-fitting during the VLBI data reduction process.

When, in addition to the radio, optical observations are available that peak in the light curve, this optical emission can be modeled as the synchrotron emission of a point source ejected in the perturbed beam, see Britzen et al. (2001) and Lobanov & Roland (2005). This short burst of very energetic relativistic $e^{\pm}$ is followed immediately by a very long burst of less energetic relativistic $e^{\pm}$. This long burst is modeled as an extended structure along the beam and is responsible for the VLBI radio emission. In that case the origin t_o of the VLBI component is the beginning of the first peak of the optical light curve and is not a free parameter of the model.

2.5. Parameters of the model

In this section, we list the possible free parameters of the model. They are

- i_o the inclination angle;
- ϕ_o the phase of the precession at $t = 0$;
- $\Delta\Xi$ the rotation angle in the plane perpendicular to the line of sight (see Eqs. (1) and (2));
- Ω the opening angle of the precession cone;
- R_o the maximum amplitude of the perturbation;
- T_p the precession period of the accretion disk;
- T_d the characteristic time for the damping of the beam perturbation;
- M_1 the mass of the black hole ejecting the radio jet;
- M_2 the mass of the secondary black hole;
- γ_c the bulk Lorentz factor of the VLBI component;
- ψ_o the phase of the BBH system at $t = 0$;
- T_b the period of the BBH system;
- t_o the time of the origin of the ejection of the VLBI component;
- V_a the propagation speed of the perturbations;
- n_{rad} is the number of steps to describe the extension of the VLBI component along the beam;
- ΔW and ΔN the possible offsets of the origin of the VLBI component.

We will see that the parameter V_a can be used to study the degeneracy of the solutions, so we can keep it constant to find the solution. The range of values that we study for parameter V_a is $0.01 \times c \le V_a \le 0.45 \times c$[2].

The parameter n_{rad} is known when the size of the VLBI component is known.

This means that, pratically, the problem we have to solve is a 15 free parameter problem.

We have to investigate the different possible scenarios with regard to the sense of the rotation of the accretion disk and the sense of the orbital rotation of the BBH system. These possibilities correspond to $\pm\,\omega_p(t - z/V_a)$ and $\pm\,\omega_b(t - z/V_a)$. Because the sense of the precession is always opposite to the sense of the orbital motion (Katz 1997), we study the two cases denoted by $+-$ and $-+$, where we have $\omega_p(t - z/V_a)$, $-\omega_b(t - z/V_a)$ and $-\omega_p(t - z/V_a)$, $\omega_b(t - z/V_a)$, respectively.

3. Method for solving the problem

3.1. Introduction

In this section, we explain the method for fitting VLBI observations using either a precession model or a BBH system model. The software is freely available on request to J. Roland[3].

This method is a practical one that provides solutions, but the method is not unique and does not guarantee that all possible solutions are found.

We calculate the projected trajectory on the plane of the sky of an ejected component and determine the parameters of the model to simultaneously produce the best fit with the observed west and north coordinates. The parameters found minimize

$$\chi_t^2 = \chi^2(W_c(t)) + \chi^2(N_c(t)), \tag{17}$$

where $\chi^2(W_c(t))$ and $\chi^2(N_c(t))$ are the χ^2 calculated by comparing the VLBI observations with the calculated coordinates $W_c(t)$

[2] We limit ourselves to nonrelativistic hydrodynamics in this model.

[3] roland@iap.fr

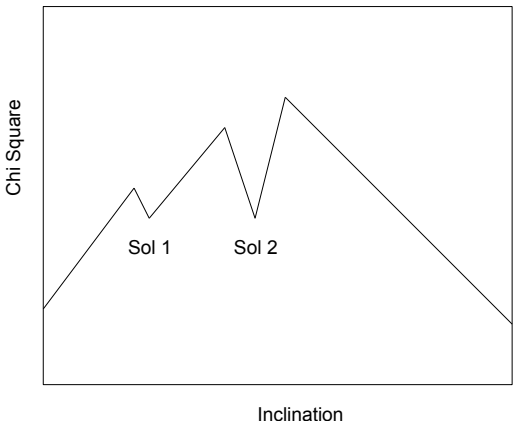

Fig. 5. Example of a possible profile of the solution $\chi^2(i_o)$. There are two possible solutions for which $\chi^2(\mathrm{Sol1}) \approx \chi^2(\mathrm{Sol2})$. They correspond to the concave parts of the surface $\chi^2(i_o)$. However, solution 2 is more robust than solution 1, i.e. it is the deepest one, and it will be the solution we adopt.

and $N_c(t)$ of the component. For instance, to find the inclination angle that provides the best fit, we minimize $\chi^2_t(i_o)$.

A good determination of the 1σ (standard deviation) error bar can be obtained using the definition

$$(\Delta i_o)_{1\sigma} = |i_o(\chi^2_{\min} + 1) - i_o(\chi^2_{\min})|, \quad (18)$$

which provides two values $(\Delta i_o)_{1\sigma+}$ and $(\Delta i_o)_{1\sigma-}$ (see Lampton et al. 1976 and Hébrard et al. 2002).

The concave parts of the surface $\chi^2(i_o)$ contain a minimum. We can find solutions without a minimum; they correspond to the convex parts of the surface $\chi^2(i_o)$ and are called mirage solutions.

To illustrate the properties of the surface $\chi^2(i_o)$ we plot in Fig. 5 a possible example of a profile of the solution $\chi^2(i_o)$. In Fig. 5, there are two possible solutions for which $\chi^2(\mathrm{Sol1}) \approx \chi^2(\mathrm{Sol2})$, solution 2 is more robust than solution 1, i.e. it is the deepest one, and it will be the solution we will keep.

We define the robustness of the solution as the square root of the difference between the smallest maximum close to the minimum and the minimum of the function χ^2. A solution of robustness 3 is a 3σ solution, i.e. $3\sigma \Leftrightarrow \Delta\chi^2 = 9$.

The main difficulties we have to solve are the following:

1. find all possible solutions;
2. eliminate the mirage solutions;
3. find the most robust solutions.

For a given inclination angle of the BBH system problem, there exists a parameter that allows us to find the possible solutions. This fundamental parameter is the ratio T_p/T_b, where T_p and T_b are the precession period of the accretion disk and the binary period of the BBH system respectively (see details in paragraph 2 of Sects. 3.3, A.4, and B.5).

Any minimum of the χ^2 function can be a local minimum and not a global minimum. However, because we investigate a wide range of the parameter T_p/T_b, namely $1 \leq T_p/T_b \leq 1000$, we expect to be able to find all possible solutions (the limit $T_p/T_b \leq 1000$ is given as an indication, in practice a limit of $T_p/T_b \leq 300$ is enough).

Note that when the solution is found, it is not unique, but there exists a family of solutions. The solution shows a degeneracy and we will see that the parameter to fix the degeneragy or to find the range of parameters that provide the family of solutions is V_a, the propagation speed of the perturbation along the beam.

Generally, for any value of the parameters, the surface $\chi^2(\lambda)$ is convex and does not present a minimum. Moreover, when we are on the convex part of the surface $\chi^2(\lambda)$, one of the important parameters of the problem can diverge. The two important parameters of the problem that can diverge are

1. the bulk Lorentz factor of the $e^{\pm}$ beam, which has to be $\gamma_b \leq 30$. This limit is imposed by the stability criterion for the propagation of the relativistic beam in the subrelativistic $e^- - p$ jet;
2. the total mass of the BBH system.

The most frequent case of divergence we can find corresponds to $\gamma_b \to \infty$. These mirage solutions are catastrophic and must be rejected. As we will see, generally, we have to study the robustness of the solution in relation to the parameters T_p/T_b, M_1/M_2, γ and i_o.

3.2. Solution of the precession model

In a first step, we fit a simple precession model without a BBH system. This corresponds to the precession induced by a spinning BH (Lense-Thirring effect) or by the magnetically driven precession (Caproni et al. 2006). This has the advantage of determining whether the solution corresponds to case I or to case II and of preliminarily determining the inclination angle and the bulk Lorentz factor of the ejected component.

We have to investigate the different possible scenarios with regard to the sense of the rotation of the accretion disk. These possibilities correspond to $\pm\omega_p(t - z/V_a)$. Accordingly, we study the two cases.

Assuming a simple precession model, these are the steps to fit the coordinates $X(t)$ and $Y(t)$ of a VLBI component:

1. *Determining the solution $\chi^2(i_o)$ and the time origin of the component ejection.* In this section we assume that $V_a = 0.1c$ (as $\chi^2(V_a)$ remains constant when V_a varies, any value of V_a can be used, see details in the next paragraph). We calculate $\chi^2(i_o)$, i.e., we minimize $\chi^2_t(i_o)$ when the inclination angle varies gradually between two values. At each step of i_o, we determine each free parameter λ such that $\partial\chi^2_t/\partial\lambda = 0$.
   Firstly, the important parameter to determine is the time origin of the ejection of the VLBI component. We compare the times of the observed peak flux with the modeled peak flux. The time origin is obtained when the two peak fluxes occur at the same time. The solutions corresponding to case II show a significant difference between the time origin of the ejection of the VLBI component deduced from the fit of the peak flux and the time origin obtained from the interpolation of the core separation.
   Second, we can make a first determination of the inclination angle and of the bulk Lorentz factor.
2. *Determining the family of solutions.* The solution previously found is not unique and shows a degeneracy. The parameter V_a can be used to study the degeneracy of the solution. Indeed, if we calculate $\chi^2(V_a)$ when V_a varies, we find that $\chi^2(V_a)$ remains constant. For the inclination angle found in the previous section and the parameters of the corresponding solution, we calculate $\chi^2(V_a)$ when V_a varies between $0.01c \leq V_a \leq 0.45c$ and deduce the range of the precession period.
3. *Determining the possible offset of the origin of the VLBI component.* In this section, we keep $V_a = 0.1c$ and using the inclination angle previously found and the corresponding solution, we calculate $\chi^2(\Delta x, \Delta y)$ when Δx and Δy

vary (Δx and Δy are the possible offsets of the VLBI origin). Solutions corresponding to case II show a significant offset of the space origin. Note that determining the offsets of the VLBI coordinates does not depend on the value of the inclination angle.

3.3. Solution of the BBH model

We have to investigate the different possible scenarios with regard to the sense of the rotation of the accretion disk and the sense of the orbital rotation of the BBH system. Because the sense of the precession is always opposite to the sense of the orbital motion, we study the two cases where we have $\omega_p(t-z/V_a)$, $-\omega_b(t-z/V_a)$ and $-\omega_p(t-z/V_a)$, $\omega_b(t-z/V_a)$, respectively.

Assuming a BBH model, this is the method for fitting the coordinates $X(t)$ and $Y(t)$ of a VLBI component:

1. *Determining the BBH system parameters for various values of* T_p/T_b. In this section, we keep the inclination angle previously found and $V_a = 0.1c$. We determine the BBH system parameters for different values of T_p/T_b, namely $T_p/T_b = 1.01$, 2.2, 4.6, 10, 22, 46, 100, and 220 for a BBH system with $M_1 = M_2$ (these values of T_p/T_b are chosen because they are equally spaced on a logarithmic scale). Generally, the BBH systems obtained with a low value of T_p/T_b, namely $T_p/T_b = 1.01$, 2.2, or 4.6 are systems with a large radius and the BBH systems obtained with a high value of T_p/T_b, namely $T_p/T_b = 10$, 22, 46, 100, or 220 are systems with a small radius.
2. *Determining the possible solutions: the* $\chi^2(T_p/T_b)$ *– diagram.* In this section, we keep the inclination angle previously found, $V_a = 0.1c$ and $M_1 = M_2$. The crucial parameter for finding the possible solutions is T_p/T_b, i.e., the ratio of the precession period and the binary period. Starting from the solutions found in the previous section, we calculate $\chi^2(T_p/T_b)$ when T_p/T_b varies between 1 and 300. We find that the possible solutions characterized by a specific value of the ratio T_p/T_b. We note that some of the solutions can be mirage solutions, which have to be detected and excluded.
3. *Determining the possible offset of the space origin.* In this section, we keep the inclination angle previously found, $V_a = 0.1c$ and $M_1 = M_2$. Starting with the solution found in the previous section, we calculate $\chi^2(\Delta x, \Delta y)$ when Δx and Δy vary (Δx and Δy are the possible offsets of the VLBI origin). If we find that an offset of the origin is needed, we correct the VLBI coordinates by the offset to continue. Note that determining the offsets of the VLBI coordinates does not depend on the value of the inclination angle.
4. *Determining the range of possible values of* T_p/T_b. In this section, we keep $V_a = 0.1c$, $M_1 = M_2$. Previously, we found a solution characterized by a value of T_p/T_b for a given inclination. Therefore we calculate $\chi^2(i_o)$ when i_o varies with a variable ratio T_p/T_b. We obtain the range of possible values of T_p/T_b and the range of possible values of i_o.
5. *Preliminary determination of* i_o, T_p/T_b *and* M_1/M_2. In this section, we keep $V_a = 0.1c$. This section is the most complicated one and differs for solutions corresponding to case I and case II. We indicate the main method and the main results (the details are provided in Sect. A.7 for the fit of component S1 of 1823+568 solutions and in Sect. B.7 for the fit of component C5 of 3C 279). We calculate $\chi^2(i_o)$ for various values of T_p/T_b and M_1/M_2. Generally, we find that there exist critical values of the parameters T_p/T_b and M_1/M_2, which separate the domains for which the solutions exist or become mirage solutions. The curves $\chi^2(i_o)$ show a minimum for given values $(i_o)_{min}$ and if necessary, we study the robustness of the solution in relation to the parameter γ, therefore we calculate $\chi^2(\gamma)$ at $i_o = (i_o)_{min}$ for the corresponding values of T_p/T_b and M_1/M_2. When these critical values are obtained, we find the domains of T_p/T_b and M_1/M_2, which produce the solutions whose robustness is greater than 1.7σ and the corresponding inclination angle i_o.
6. *Determining a possible new offset correction.* Using the solution found in the previous section, we calculate again $\chi^2(\Delta x, \Delta y)$ when Δx and Δy vary. When a new offset of the origin is needed, we correct the VLBI coordinates by the new offset to continue. Note that this new offset correction is smaller than the first one found previously.
7. *Characteristics of the final solution to the fit of the VLBI component.* We are now able to find the BBH system parameters that produce the best solution for the fit with the same method as described in point 5, *Preliminary determination of* i_o, T_p/T_b *and* M_1/M_2.
8. *Determining the family of solutions.* The solution previously found is not unique and shows a degeneracy. The parameter V_a can be used to study the degeneracy of the solution. Indeed, when we calculate $\chi^2(V_a)$ for varying V_a, we find that $\chi^2(V_a)$ remains constant. Using the solution found in the previous section and the parameters of the corresponding solution, we calculate $\chi^2(V_a)$ when V_a varies between $0.01c \leq V_a \leq 0.45c$ and deduce the range of the precession period, the binary period, and the total mass of the BBH system.
9. *Determining the size of the accretion disk.* Because we know the parameters of the BBH system, we can deduce the rotation period of the accretion disk and its size.

4. Method – Case I

4.1. Introduction: fitting the component S1 of 1823+568

Case I corresponds to a VLBI component ejected either from the VLBI core or to one where the offset of the origin of the ejection is smaller than or on the order of the smallest error bars of the VLBI component coordinates. It is the simplest case to solve. To illustrate the method of solving the problem corresponding to case I, we fit the component S1 of the source 1823+568 (Figs. 6 and 7).

4.2. VLBI data of 1823+568

1823+568 is an quasar at a redshift of 0.664 ± 0.001 (Lawrence et al. 1986). The host galaxy is elliptical according to HST observations (Falomo et al. 1997). The jet morphology on kpc-scales is complex – a mirrored S in observations with the MTRLI at 1666 MHz and with the VLA at 2 and 6 cm (O'Dea et al. 1988). The largest extension of 1823+568 is 15″, corresponding to 93 kpc. On pc-scales the jet is elongated and points in a southern direction from the core (Pearson & Readhead 1988) – in accordance with the kpc-structure. Several components could be identified in the jet, e.g., Gabuzda et al. (1989) and Gabuzda et al. (1994), Gabuzda & Cawthorne (1996), Jorstad et al. (2005). A VSOP Space VLBI image of 1823+568 has been obtained by Lister et al. (2009a). All identified components show strong polarization. The linear polarization is parallel to the jet ridge direction. Most of the components show slow apparent superluminal motion. The fast component S1 moved with an apparent velocity of about $20c \pm 2c$ until 2005 and subsequently decreases (Glück 2010). Twenty-two VLBA observations obtained

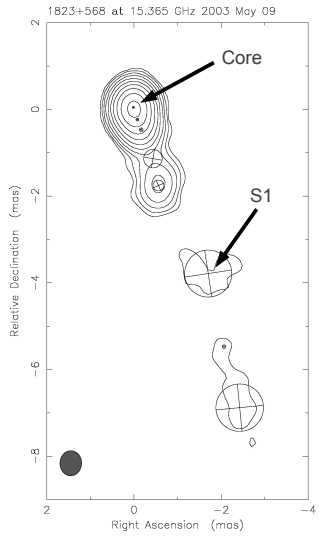

Fig. 6. 15 GHz natural weighted VLBI image of 1823+568 with fitted circular Gaussian components observed 9 May 2003 (Glück 2010). The map peak flux density was 1.27 Jy/beam, where the convolving beam was 0.58 × 0.5 mas at position angle (PA) −2.09°. The contour levels were drawn at 0.15, 0.3, 0.6, 1.2, 2.4, 4.8, 9.6, 19.2, 38.4, and 76.8% of the peak flux density.

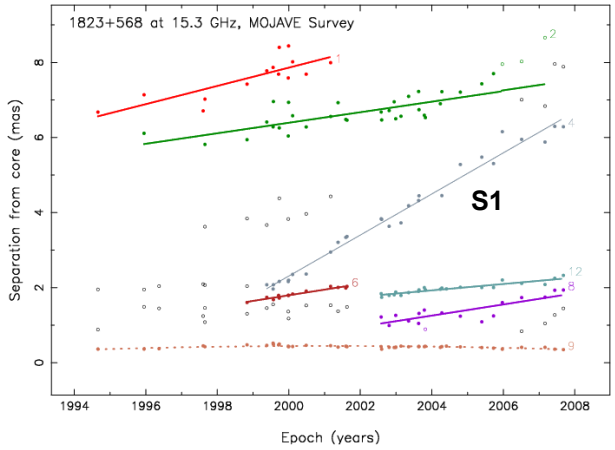

Fig. 7. Separation from the core for the different VLBI components for the source 1823+568 from MOJAVE data (Lister et al. 2009b). For details concerning the plot and the line fits see Lister et al. (2009b). We fit component S1 corresponding to component 4 from the MOJAVE survey. Component S1 moves fast, which may indicate that two families of VLBI components exist in the case of 1823+568. If this is the case, the nucleus of 1823+568 could contain a BBH system.

at 15 GHz within the 2-cm MOJAVE survey between 1994.67 and 2010.12 have been re-analyzed and model-fitted to determine the kinematics of the individual components. For details of the data reduction and analysis see Glück (2010).

The radio map of 1823+568, observed 9 May 2003, is shown in Fig. 6. The data are taken from Glück (2010).

4.3. Preliminary remarks

The redshift of the source is $z_s \approx 0.664$, and using for the Hubble constant $H_o \approx 72$ km/s/Mpc, the luminosity distance of the source is $D_l \approx 3882$ Mpc and the angular distance is $D_a = D_l/(1+z)^2$.

For details of the values of the data and of their error bars see Glück (2010). At 15 GHz, calling the beam size *Beam*, we adopted for the minimum values Δ_{min} of the error bars of the observed VLBI coordinates, the values in the range:

$$Beam/15 \leq \Delta_{min} \leq Beam/12, \quad (19)$$

see Sect. C for details concerning this choice.

For 1823+568, observations were performed at 15 GHz and the beam size is mostly circular and equal to $Beam \approx 0.5$ mas. We adopted as minimum values of the error bars the values $(\Delta W)_{min} \approx Beam/12 \approx 40$ μas and $(\Delta N)_{min} \approx Beam/12 \approx 40$ μas for the west and north coordinates of component S1, i.e., when the error bars obtained from the VLBI data reduction were smaller than $(\Delta W)_{min}$ or $(\Delta N)_{min}$, they were enlarged to the minimum values. The minimum values were chosen empirically, but the adopted values were justified a posteriori by comparing the χ^2 value of the final solution and the number of constraints to make the fit and to obtain a reduced χ^2 close to 1. For the component S1, we have $(\chi^2)_{final} \approx 51$ for 56 constraints, the reduced χ^2 is $\chi^2_r = (\chi^2)_{final}/56 \approx 0.91$. Lister & Homan (2005) suggested that the positional error bars should be about 1/5 of the beam size. However, if we had chosen $(\Delta W)_{min} = (\Delta N)_{min} \approx Beam/5 \approx 100$ μas, we would have $(\chi^2)_{final} \ll 56$, indicating that the minimum error bars would be overestimated (see details in Sect. C).

To obtain a constant projected trajectory of the VLBI component in the plane perpendicular to the line of sight, the integration step to solve Eq. (10) changes when the inclination angle varies. The integration step was $\Delta t = 0.8$ yr when $i_o = 5°$. When i_o varied, it was $\Delta t = 0.8(\sin(5°)/\sin(i_o))$ yr.

The trajectory of component S1 is not long enough to constrain the parameter T_d, i.e., the characteristic time for the damping of the beam perturbation. We fit assuming that $T_d \leq 2500$ yr; this value produced a good trajectory shape.

The time origin of the ejection of the component S1, deduced from the interpolation of VLBI data, is $t_o \approx 1995.6$ (Fig. 7).

Close to the core, the size of S1 is ≈0.24 mas, therefore we assumed that $n_{rad} = 75$, where n_{rad} is the number of steps to describe the extension of the VLBI component along the beam. At $i_o = 5°$ with an integration step $\Delta t = 0.8$ yr, we calculated the length of the trajectory corresponding to each integration step. The size of the component is the sum of the first $n_{rad} = 75$ lengths.

4.4. Final fit of component S1 of 1823+568

Here we present the solution to the fit of S1, the details for the fit can be found in Sect. A.

We studied the two cases $\pm\omega_p(t - z/V_a)$. The final solution of the fit of component S1 using a BBH system corresponds to $+\omega_p(t - z/V_a)$ and $-\omega_b(t - z/V_a)$.

The main characteristics of the solution of the BBH system associated with 1823+568 are that

- the radius of the BBH system is $R_{bin} \approx 60$ μas ≈ 0.42 pc;
- the VLBI component S1 is not ejected by the VLBI core, and the offsets of the observed coordinates are $\Delta W \approx +5$ μas and $\Delta N \approx 60$ μas;
- the ratio T_p/T_b is $8.88 \leq T_p/T_b \leq 9.88$; and
- the ratio M_1/M_2 is $0.095 \leq M_1/M_2 \leq 0.25$.

The results of the fits obtained for $T_p/T_b = 8.88$ and $T_p/T_b = 9.88$ are given in Sect. A.9. The solutions found with $T_p/T_b \approx 8.88$ are slightly more robust, but both solutions can be used.

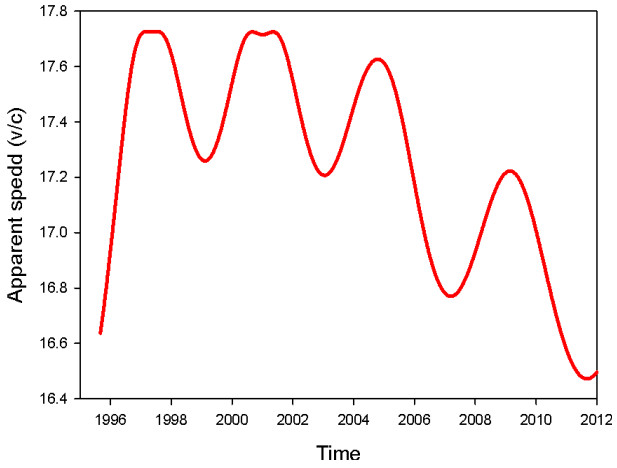

Fig. 8. Apparent speed of component S1 increases at the begining, then it is ≈17.5c until 2005, and finally, it decreases slowly assuming a constant bulk Lorentz factor $\gamma_c \approx 17.7$.

To continue, we arbitrarily adopted the solution with $T_p/T_b \approx 8.88$ and $M_1/M_2 \approx 0.17$. We deduced the main parameters of the model, which are that

- the inclination angle is $i_o \approx 3.98°$;
- the angle between the accretion disk and the rotation plane of the BBH system is $\Omega \approx 0.28°$ (this is also the opening angle of the precession cone);
- the bulk Lorentz factor of the VLBI component is $\gamma_c \approx 17.7$; and
- the origin of the ejection of the VLBI component is $t_o \approx 1995.7$.

The variations of the apparent speed of component S1 are shown in Fig. 8.

We can determine the Doppler factor (Eq. (12)), and consequently, we can estimate the observed flux density (Eq. (13)). This was used to fit the temporal position of the peak flux and to determine the temporal origin of the ejection of the VLBI component (see Sect. A.1 for the details).

The fit of the two coordinates $W(t)$ and $N(t)$ of the component S1 of 1823+568 is shown in Fig. 9. The points are the observed coordinates of component S1 that were corrected by the offsets $\Delta W \approx +5$ μas and $\Delta N \approx 60$ μas, and the red lines are the coordinates of the component trajectory calculated using the BBH model assuming the solution parameters, i.e., $T_p/T_b \approx 8.88$, $M_1/M_2 \approx 0.17$, $i_o \approx 3.98°$, etc.

Finally, we compared this solution with the solution obtained using the precession model. The $\chi^2_{min}(i_o)$ is about 51 for the fit using the BBH system and about 67 for the precession model (see Sect. A.1), i.e., the BBH system solution is a 4σ better solution. To fit the ejection of component S1 we used 56 observations (the west and north coordinates corresponding to the 28 epochs of observation), so the reduced χ^2 is $\chi^2_r = 51/56 \approx 0.91$, indicating that the minimum values used for the error bars are correct.

4.5. Determining the family of solutions

For the inclination angle previously found, i.e., $i_o \approx 3.98°$, $T_p/T_b \approx 8.88$, $M_1/M_2 \approx 0.17$, and $R_{bin} \approx 60$ μas, we gradually varied V_a between 0.01c and 0.45c. The function $\chi^2(V_a)$ remained constant, indicating a degeneracy of the solution. We deduced the range of variation of the BBH system parameters. They are given in Table 1.

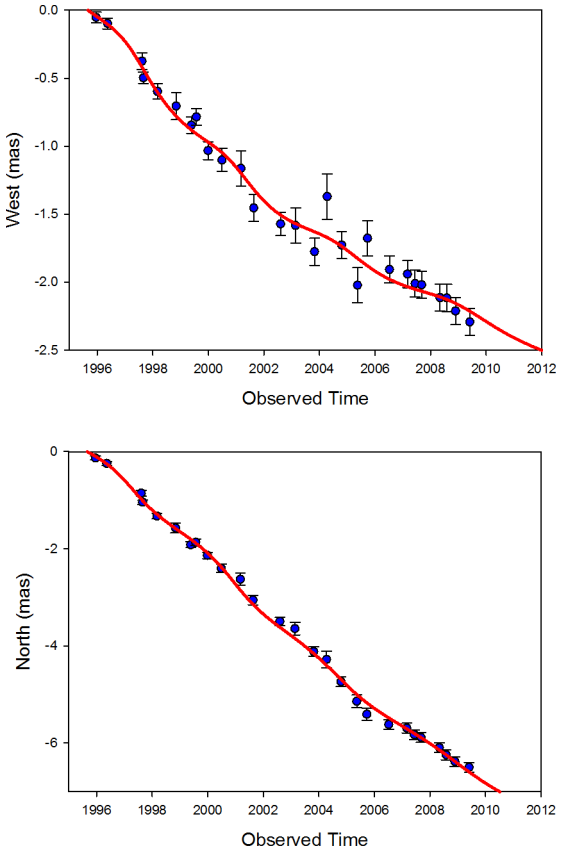

Fig. 9. Fit of the two coordinates $W(t)$ and $N(t)$ of component S1 of 1823+568. They correspond to the solution with $T_p/T_b \approx 8.88$, $M_1/M_2 \approx 0.17$, and $i_o \approx 3.98°$. The points are the observed coordinates of component S1 that were corrected by the offsets $\Delta W \approx +5$ μas and $\Delta N \approx 60$ μas (the VLBI coordinates and their error bars are taken from Glück 2010). The red lines are the coordinates of the component trajectory calculated using the BBH model.

The period of the BBH system is not obviously related to a possible periodicity of the radio or the optical light curve.

4.6. Determining the size of the accretion disk

From the knowledge of the mass ratio $M_1/M_2 \approx 0.17$ and the ratio $T_p/T_b \approx 8.88$, we calculated in the previous section the mass of the ejecting black hole M_1, the orbital period T_b, and the precession period T_p for each value of V_a.

The rotation period of the accretion disk, T_{disk}, is given by (Britzen et al. 2001)

$$T_{disk} \approx \frac{4}{3}\frac{M_1 + M_2}{M_2} T_b \frac{T_b}{T_p}. \quad (20)$$

Thus we calculated the rotation period of the accretion disk, and assuming that the mass of the accretion disk is $M_{disk} \ll M_1$, the size of the accretion disk R_{disk} is

$$R_{disk} \approx \left(\frac{T^2_{disk}}{4\pi^2} G M_1\right)^{1/3}. \quad (21)$$

We found that the size of the accretion disk does not depend on V_a and is $R_{disk} \approx 0.090$ pc ≈ 0.013 mas.

Table 1. Ranges for the BBH system parameters.

V_a	$0.01c$	$0.45c$
$T_p(V_a)$	≈540 000 yr	≈6700 yr
$T_b(V_a)$	≈60 600 yr	≈750 yr
$(M_1 + M_2)(V_a)$	$\approx 1.6 \times 10^5\ M_\odot$	$\approx 1.05 \times 10^9\ M_\odot$

5. The method – Case II

5.1. Introduction: application to component C5 of 3C 279

Case II corresponds to an ejection of the VLBI component with an offset of the origin of the component larger than the smallest error bars of the VLBI component coordinates. This is the most difficult case to solve because data have to be corrected by an unknown offset That is larger than the smallest error bars.

When we apply the precession model, there are two signatures of case II, which are

1. the problem of the time origin of the VLBI component, and
2. the shape of the curve $\chi^2_t(i_o)$.

Using the precession model, we modeled the flux and compared the time position of the first peak flux with the time position of the observed peak flux. If the origin time deduced from interpolating the VLBI data was very different than the origin time deduced from the precesion model, we concluded that there is a time origin problem (see Sect. B.1). We show that this origin-time problem is related to the offset of the space origin of the VLBI component, i.e., the VLBI component is not ejected by the VLBI core and this offset is larger than the smallest error bars (see Sect. B.3).

When the offset of the space origin is larger than the smallest error bars of the component positions and the VLBI coordinates are not corrected by this offset, the curve $\chi^2_t(i_o)$ can have a very characteristic shape:

1. the inclination angle is limited to a specific interval, i.e., $i_{min} \le i_o \le i_{max}$;
2. when $i_o \to i_{max}$ and when $i_o \to i_{min}$, the bulk Lorentz factor of the VLBI component diverges, i.e., $\gamma_c \to \infty$; and
3. the function $\chi^2_t(i_o)$ does not have a minimum in the interval $i_{min} \le i_o \le i_{max}$.

See Fig. B.1 corresponding to the precession model applied to component C5 of 3C 279.

5.2. MOJAVE data of 3C 279

The radio quasar 3C 279 ($z = 0.536$ Marziani et al. 1996) is one of the brightest extragalactic radio sources and has been observed and studied in detail for decades. Superluminal motion in the outflow of the quasar was found by Whitney et al. (1971) and Cohen et al. (1971). Thanks to the increasing resolution and sensitivity of modern observation techniques, a more complex picture of 3C 279 appeared, including multiple superluminal features moving along different trajectories downstream the jet (Unwin et al. 1989). The apparent speed of these components span an interval between $4c$ and $16c$ (Cotton et al. 1979; Wehrle et al. 2001).

We used the MOJAVE observations of 3C 279 (Lister et al. 2001). Seventy-six VLBA observations obtained at 15 GHz within the 2-cm MOJAVE survey between 1999.25 and 2007.64 were re-analyzed and model-fitted to determine the coordinates of the VLBI components. We used the NRAO Astronomical Image Processing System (AIPS) to calibrate the data. We performed an amplitude calibration and applied a correction for the atmospheric opacity for the high-frequency data ($\nu > 15$ GHz). The parallactic angle correction was taken into account before we calibrated the phases using the pulse-scale signal and a final fringe fit. The time- and frequency-averaged data were imported to DIFMAP (Shepherd 1997), were we used the CLEAN and MODELFIT algorithm for imaging and model fitting, respectively.

The fully calibrated visibilities were fitted in DIFMAP using the algorithm MODELFIT and 2D circular Gaussian components. These components were characterized by their flux density, S_{mod}, position r_{mod}, position angle (PA), θ_{mod} (measured from north through east), and their full-width at half-maximum (FWHM). Since the number of fitted Gaussians was initially not limited, we only then added a new component when the χ^2 value decreased significantly. This approach led to a minimum number of Gaussians that can be regarded as a reliable representation of the source. We modeled each epoch separately to avoid biasing effects. The kinematics of the source could thus be analyzed by tracking the fitted components. The average beam for the 15 GHz observations is 0.51 mas × 1.34 mas.

The radio map of 3C 349, observed 15 june 2003, is shown in Fig. 10. The data are taken from Lister et al. (2009a).

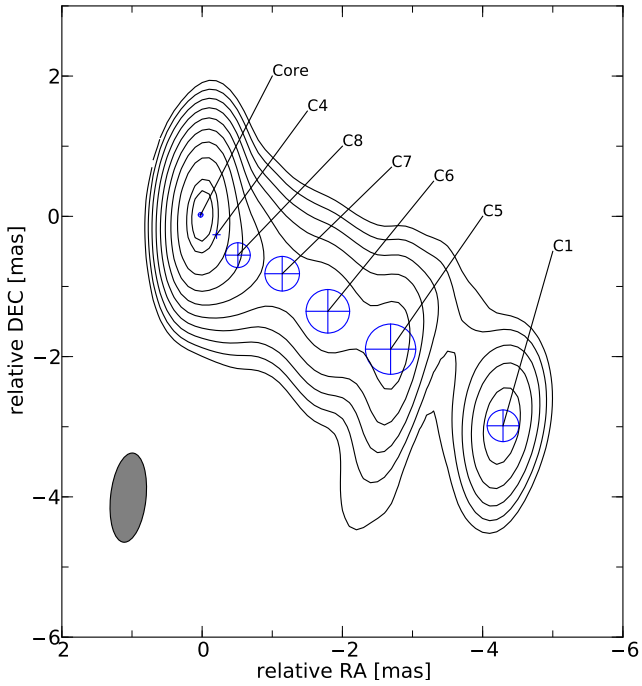

Fig. 10. 15 GHz natural-weighted VLBI image of 3C 279 with fitted circular Gaussian components observed 15 June 2003 (Lister et al. 2009a). The map peak flux density was 8.3 Jy/beam, where the convolving beam was 1.3×0.5 mas at position angle (PA) −6.0°. The contour levels were drawn at 0.2, 0.5, 1.0, 2.0, 4.0, 8.0, 16, 32, 64, and 80% of the peak flux density. Component C4 is a stationary component (see Fig. 11).

5.3. Preliminary remarks

The redshift of 3C 279 is $z \approx 0.536$, and using for the Hubble constant $H_o \approx 72$ km/s/Mpc, the luminosity distance of the source is $D_l \approx 3070$ Mpc and the angular distance is $D_a = D_l/(1+z)^2$.

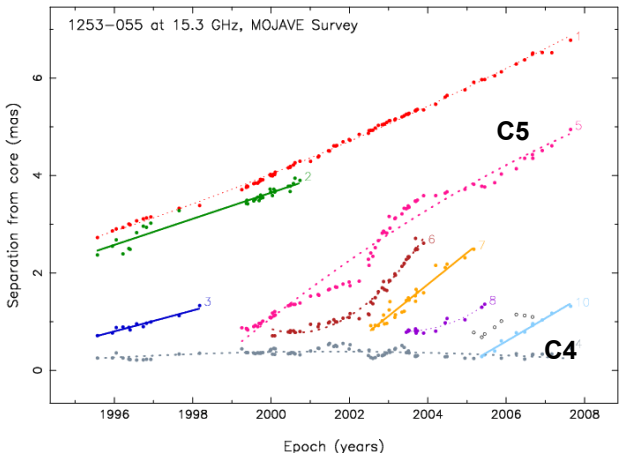

Fig. 11. Separation from the core for the different VLBI components for the source 3C 279 from MOJAVE data (Lister et al. 2009b). For the obtaining of the plotted line fits see Lister et al. (2009b). We fit component C5. Component C5 is ejected from an origin with a large offset from the VLBI core.

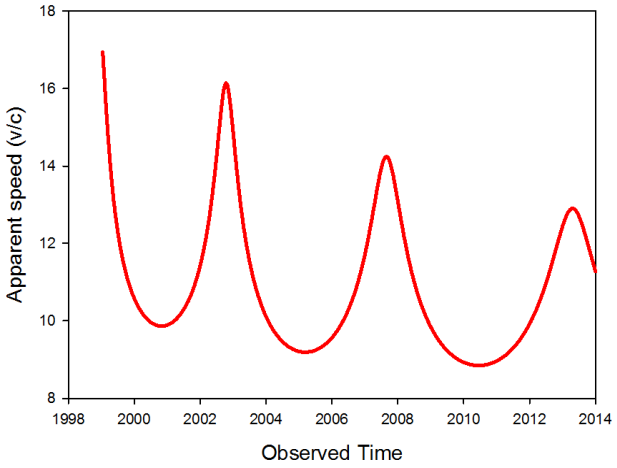

Fig. 12. Apparent speed of component C5 varies between $17c$ and $9c$ assuming a constant bulk Lorentz factor $\gamma_c \approx 16.7$.

For details of the values of the data see Lister et al. (2009a). Because the observations were performed at 15 GHz and the beam size was 0.51 mas×1.34 mas, we adopted for the minimum values of the error bars the values $(\Delta W)_{\rm min} \approx Beam/15 \approx 34\ \mu$as and $(\Delta N)_{\rm min} \approx Beam/15 \approx 89\ \mu$as for the west and north coordinates of component C5. The adopted values were justified a posteriori by comparing the χ^2 value of the final solution and the number of constraints to make the fit and to obtain a reduced χ^2 close to 1. For the component C5, we have $(\chi^2)_{\rm final} \approx 150$ for 152 constraints, thus the reduced χ^2 is: $(\chi^2)_{\rm r} \approx 0.99$. It has been suggested by Lister & Homan (2005) that the positional error should be within 20% of the convolving beam size, i.e., $\approx Beam/5$. See Sect. C for details concerning the choice adopted in this article and the determination of the χ^2, the characteristics of the solution using minimum erros bars are as large as $\approx Beam/5$.

The integration step used to solve Eq. (10) is $\Delta t = 0.8$ yr when $i_{\rm o} = 5°$. When $i_{\rm o}$ varies, it is $\Delta t = 0.8(\sin(5°)/\sin(i_{\rm o}))$ yr.

The trajectory of component C5 is not long enough to constrain the parameter $T_{\rm d}$, i.e., the characteristic time for the damping of the beam perturbation. We fit assuming that $T_{\rm d} \leq 2000$ yr.

The time origin of the ejection of the component C5 cannot be deduced easily from the interpolation of VLBI data (Lister et al. 2009b). However, we show in Sect. B.1 how, using the precession model, it is possible to obtain the minimum time origin of the VLBI component by comparing the time position of the calculated first peak flux with the observed time position of the first peak flux.

Close to the core, the size of C5 is ≈0.25 mas, therefore we assumed that $n_{\rm rad} = 75$, where $n_{\rm rad}$ is the number of steps to describe the extension of the VLBI component along the beam.

5.4. Final fit of component C5 of 3C 279

Here we present the solution to the fit of C5, the details for the fit can be found in Sect. B. The fit of component C5 using a BBH system corresponds to $-\omega_{\rm p}(t - z/V_a)$ and $+\omega_{\rm b}(t - z/V_a)$.

The main characteristics of the solution of the BBH system associated with 3C 279 are that

- the radius of the BBH system is $R_{\rm bin} \approx 420\ \mu$as ≈ 2.7 pc;
- the VLBI component C5 is not ejected by the VLBI core and the offsets of the observed coordinates are $\Delta W \approx +405\ \mu$as and $\Delta N \approx +110\ \mu$as;
- the ratio $T_{\rm p}/T_{\rm b}$ is $T_{\rm p}/T_{\rm b} \approx 140$; and
- the ratio M_1/M_2 is $M_1/M_2 \approx 2.75$.

The results of the fits obtained for $T_{\rm p}/T_{\rm b} \approx 140$ and $M_1/M_2 \approx 2.75$ are given in Appendix B.9.

Adopting the solution with $T_{\rm p}/T_{\rm b} \approx 140$ and $M_1/M_2 \approx 2.75$, we deduced the main parameters of the model.

- The inclination angle is $i_{\rm o} \approx 10.4°$.
- The angle between the accretion disk and the rotation plane of the BBH system is $\Omega \approx 2.4°$ (this is also the opening angle of the precession cone).
- The bulk Lorentz factor of the VLBI component is $\gamma_{\rm c} \approx 16.7$.
- The origin of the ejection of the VLBI component is $t_{\rm o} \approx 1999.0$.

The variations of the apparent speed of component C5 are shown in Fig. 12.

We can determine the Doppler factor (Eq. (12)), and consequently we can estimate the observed flux density (Eq. (13)). Using the precession model, we fitted the temporal position of the peak flux and determined the temporal origin of the ejection of the VLBI component (see Sect. B.1 for the details). Using the BBH model, we calculated and plotted in Fig. 13 the flux variations of C5 using Eq. (A.1). We found that the time origin of the ejection of component C5 is $t_{\rm o} \approx 1999.03$. Although Eq. (A.1) is a rough estimate of the flux density variations, it allows us

- to check the time origin of the ejection of the VLBI component found using the BBH model;
- to compare the time positon of the modeled first peak flux with the observed first peak flux;
- to obtain a good shape of the variation of the flux density during the first few years and explain the difference between the radio and the optical light curves. In some cases, in addition to the radio, optical observations show a light curve with peaks separated by about one year, see for instance the cases of 0420-016 (Britzen et al. 2001) and 3C 345 (Lobanov & Roland 2005). Using Eq. (A.1), the optical emission can be modeled as the synchrotron emission of a point source ejected in the perturbed beam (Britzen et al. 2001; Lobanov & Roland 2005). This short burst of very energetic relativistic $e^{\pm}$ is followed immediately by a very long burst of less

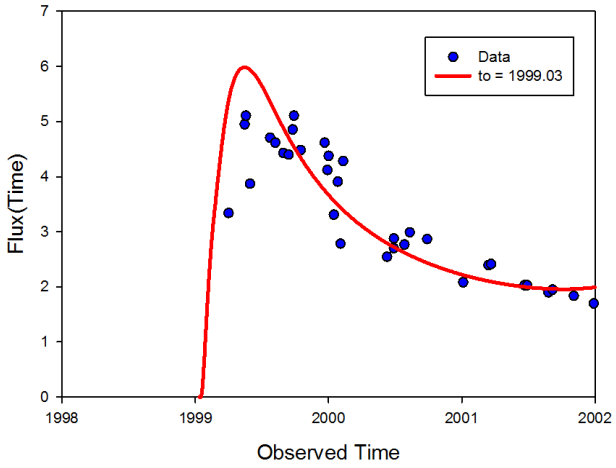

Fig. 13. Flux variations of component C5 using the BBH model. The time origin of the ejection of C5 is 1999.03.

Table 2. Ranges for the BBH system parameters.

V_a	$0.01c$	$0.45c$
$T_p(V_a)$	$\approx 3.12 \times 10^6$ yr	$\approx 38\,500$ yr
$T_b(V_a)$	$\approx 22\,300$ yr	≈ 275 yr
$(M_1 + M_2)(V_a)$	$\approx 3.2 \times 10^8\ M_\odot$	$\approx 213 \times 10^{10}\ M_\odot$

energetic relativistic $e^{\pm}$. This long burst is modeled as an extended structure along the beam and is responsible for the VLBI radio emission.

The fit of both coordinates $W(t)$ and $N(t)$ of component C5 of 3C 279 are shown in Fig. 14. The points are the observed coordinates of component C5 that were corrected for the offsets $\Delta W \approx +405$ μas and $\Delta N \approx +110$ μas, the red lines are the coordinates of the component trajectory calculated using the BBH model assuming the solution parameters, i.e., $T_p/T_b \approx 140$, $M_1/M_2 \approx 2.75$, $i_o \approx 10.4°$, etc.

Finally, we compared this solution with the solution obtained using the precession model. The $\chi^2_{min}(i_o)$ is about 151.4 for the fit using the BBH system and >1000 for the precession model (see Sect. B.1). To fit the ejection of component C5 we used 152 observations (76 epochs), so the reduced χ^2 is $\chi^2_r = \chi^2_{min}/152 \approx 0.996$.

5.4.1. Determining the family of solutions

The solution is not unique, but there exists a family of solutions. For the inclination angle previously found, i.e., $i_o \approx 10.4°$ and using the parameters of the corresponding solution, i.e., $T_p/T_b \approx 140$, $M_1/M_2 \approx 2.75$ and $R_{bin} \approx 420$ μas, we gradually varied V_a between $0.01c$ and $0.45c$. The function $\chi^2(V_a)$ remains constant, indicating a degeneracy of the solution, and we deduced the range of variation of the BBH system parameters. They are given in Table 2.

5.4.2. Determining the size of the accretion disk

From the knowledge of the mass ratio $M_1/M_2 \approx 2.75$ and the ratio $T_p/T_b \approx 140$, we calculated in the previous section the mass of the ejecting black hole M_1, the orbital period T_b, and the precession period T_p for each value of V_a.

We calculated the rotation period of the accretion disk, T_{disk}, using (20). Assuming that the mass of the accretion disk is

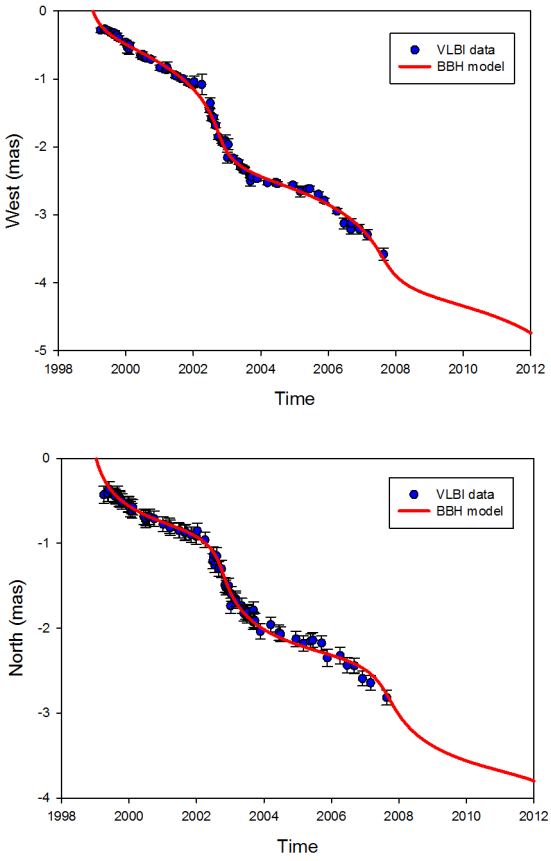

Fig. 14. Fit of the two coordinates $W(t)$ and $N(t)$ of component C5 of 3C 279. They correspond to the solution with $T_p/T_b \approx 140$, $M_1/M_2 \approx 2.75$, and $i_o \approx 10.4°$. The points are the observed coordinates of component C5 that were corrected for the offsets $\Delta W \approx +405$ μas and $\Delta N \approx +110$ μas. VLBI coordinates are taken from Lister et al. (2009a). The red lines are the coordinates of the component trajectory calculated using the BBH model.

$M_{disk} \ll M_1$, the size of the accretion disk R_{disk} is calculated using (21).

We found that the size of the accretion disk does not depend on V_a and is $R_{disk} \approx 0.26$ pc ≈ 0.041 mas.

5.4.3. Comparing of the trajectories of C5 and C10

We see from Fig. 11 that

- components C5 and C6 probably follow probably the same trajectories;
- component C10 follows a different trajectory than C5 and C6.

Thus, using the MOJAVE data (Lister et al. 2009b), we plot in Fig. 15 the trajectories of C5 and C10. We found that

- component C10 is probably ejected by the VLBI core;
- component C5 is ejected with a large offset from the VLBI core; and
- components C5 and C10 follow two different trajectories and are not ejected from the same origins, indicating that the nucleus of 3C 279 contains a BBH system.

6. Discussion and conclusion

We showed how from the knowledge of the coordinates *West*(t) and *North*(t) of the ejected VLBI component one can find the

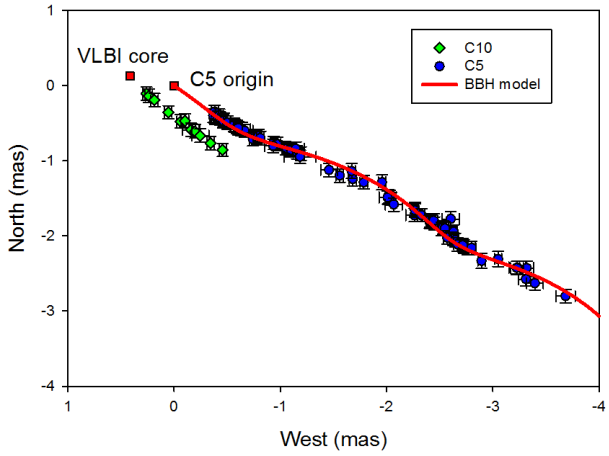

Fig. 15. Using the MOJAVE data (Lister et al. 2009b), we plot the trajectories of C5 and C10. Component C10 is probably ejected by the VLBI core and component C5 is ejected with a large offset from the VLBI core. Components C5 and C10 follow two different trajectories and are ejected from different origins, indicating that the nucleus of 3C 279 contains a BBH system. Note that the origin of this caption corresponds to the origin of the ejection of component C5, thus all MOJAVE coordinates have been corrected for the offsets $\Delta W \approx +405$ μas and $\Delta N \approx +110$ μas.

characteristics of the BBH system in both cases. To illustrate case I, we fitted component S1 of 1823+568, and to illustrate case II, we fitted component C5 of 3C 279.

From the fit of the coordinates of component S1 of 1823+568, the main characteristics of the final solution of the BBH system associated with 1823+568 are that

- the radius of the BBH system is $R_{\rm bin} \approx 60$ μas ≈ 0.42 pc;
- the VLBI component S1 is not ejected by the VLBI core, and the offsets of the observed coordinates are $\Delta W \approx +5$ μas and $\Delta N \approx 60$ μas;
- the ratio $T_{\rm p}/T_{\rm b}$ is $8.88 \leq T_{\rm p}/T_{\rm b} \leq 9.88$;
- the ratio M_1/M_2 is $0.095 \leq M_1/M_2 \leq 0.25$;
- the inclination angle is $i_{\rm o} \approx 4.0°$;
- the bulk Lorentz factor of the VLBI component is $\gamma_{\rm c} \approx 17.7$; and
- the origin of the ejection of the VLBI component is $t_{\rm o} \approx$ 1995.7.

From the fit of the coordinates of component C5 of 3C 279, the main characteristics of the final solution of the BBH system associated with 3C 279 are that

- the radius of the BBH system is $R_{\rm bin} \approx 420$ μas ≈ 2.7 pc;
- the VLBI component C5 is not ejected by the VLBI core and the offsets of the observed coordinates are $\Delta W \approx +405$ μas and $\Delta N \approx +110$ μas;
- the ratio $T_{\rm p}/T_{\rm b}$ is $T_{\rm p}/T_{\rm b} \approx 140$;
- the ratio M_1/M_2 is $M_1/M_2 \approx 2.75$;
- the inclination angle is $i_{\rm o} \approx 10.4°$;
- the bulk Lorentz factor of the VLBI component is $\gamma_{\rm c} \approx 16.7$; and
- the origin of the ejection of the VLBI component is $t_{\rm o} \approx$ 1999.0.

If, in addition to the radio observations, one can obtain optical, X-ray, or γ-ray observations that show a light curve with peaks, the simultaneous fit of the VLBI coordinates and this light curve put stronger constraints on the characteristics of the BBH system. The high-frequency emission can be modeled as the synchrotron emission or the inverse Compton emission of a point source ejected in the perturbed beam, see Britzen et al. (2001) for PKS 0420-014 and Lobanov & Roland (2005) for 3C 345. This short burst of very energetic relativistic $e^{\pm}$ is followed immediately by a very long burst of less energetic relativistic $e^{\pm}$. This long burst is modeled as an extended structure along the beam and is responsible for the VLBI radio emission. The simultaneous fit of the VLBI coordinates and the optical light curve using the same method as the one developed in this article has to be achieved.

Observations of compact radio sources in the first mas show that the VLBI ejections do not follow a straight line, and modeling the ejection shows in each case studied that the nucleus contains a BBH system. Accordingly, Britzen et al. (2001) assumed that all radio sources contain a BBH system. If extragalactic radio sources are associated with galaxies formed after the merging of galaxies and if the formation of extragalactic radio sources is related to the presence of binary black hole systems in their nuclei, we can explain

- why extragalactic radio sources are associated with elliptical galaxies;
- why more than 90% of the quasars are radio-quiet quasars, e.g., Kellermann et al. (1989) and Miller et al. (1990).

Radio-quiet quasars are active nuclei that contain a single black hole and can be associated with spiral galaxies (Peacock et al. 1986). Although it has not been proven yet that radio-quiet quasars only contain a single black hole, the hypothesis for distinguishing between radio-loud and radio-quiet quasars on the basis of the binarity of the central engine is supported by comparing the optical properties of the two classes (Goldschmidt et al. 1999). Recent observations of the central parts of radio galaxies and radio-quiet galaxies show a systematic difference between the two classes (Kharb et al. 2012).

Because *Gaia* will provide positions of extragalactic radio sources within ≈25 μas, the link between the *Gaia* reference frame from optical observations of extragalactic radio sources and the reference frame obtained from VLBI observations will have to take into account the complex structure of the nuclei of extragalactic radio sources, because with a resolution of ≈25 μas, probably all these sources will appear as double sources, and the radio core, obtained from VLBI observations and the optical core obtained by *Gaia* will not necessarily be the same.

We conclude, remarking that if the inner parts of the accretion disk contain a warp or precess faster than the precession of the outer part, this will produce a very small perturbation that will produce a day-to-month variability of the core flux (Roland et al. 2009).

Acknowledgements. J.R. thanks Alain Lecavelier des Etangs and Simon Prunet for useful discussions and comments. This research has made use of data from the MOJAVE database that is maintained by the MOJAVE team (Lister et al. 2009a) and part of this work was supported by the COST Action MP0905 Black Holes in a Violent Universe.

Appendix A: Fit of component S1 of 1823+568

A.1. Fit of S1 using the precession model

To fit the ejection of component S1, we used 56 observations (28 epochs).

We studied the two cases $\pm\omega_{\rm p}(t - z/V_a)$. The final solution of the fit of component S1 of 1823+568 using a BBH system

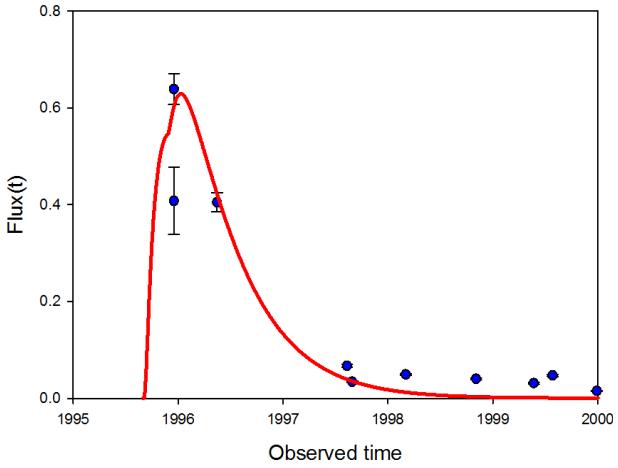

Fig. A.1. Fit of the first peak flux of component S1 of 1823+568 using the precession model. The time origin deduced from the fit of the peak flux is $t_o \geq 1995.65$ and is comparable with the time origin deduced from VLBI observations interpolation, i.e., $t_o \approx 1995.60$.

corresponds to $+\omega_p(t-z/V_a)$, therefore we discuss only this case in this appendix. In this section, we assume that $V_a = 0.1c$.

The range of inclination we explore is $0.5° \leq i_o \leq 10°$.

An important parameter for the fit is the time origin of the ejection of the VLBI component. We model the flux using equation

$$S_c = \delta_c(t)^{2+\alpha_r}/Fac \\ * \exp(-T_{opacity}/t) * \exp(-t/T_{decay}), \quad (A.1)$$

where Fac is a scaling factor, $T_{opacity}$ is the characteristic time to describe the synchrotron opacity, and T_{decay} is the characteristic time to describe the losses. This is the simplest way to model the flux and does not take into account in situ re-acceleration of the relativistic particles along the beam and synchrotron, inverse Compton, or expansion losses. We do not aim to fit the flux light curve, but we wish to compare the time position of the modeled first peak flux with the observed first peak flux (Fig. A.1). This provides the minimum for the time origin of the ejection of the VLBI component. For S1 we find $t_o \geq 1995.65$. This value agrees well with the time origin obtained from VLBI data interpolation, which is $t_o \approx 1995.60$ (Glück 2010). This case corresponds to case I, i.e., if there is an offset of the VLBI ejection, it is smaller than or on the order of the smallest error bars of the VLBI component coordinates. In the following we keep t_o as a free parameter in the range $1995.65 \leq t_o \leq 1995.90$.

Because the function $\chi^2_t(i_o)$ is mostly flat between 4 and 10 degrees, to continue we abitrarily adopted the inclination angle $i_o \approx 6°$. The main results of the fit for the precession model are that

1. the opening angle fo the precession cone is $\Omega \approx 0.46°$;
2. the bulk Lorentz factor of S1 is $\gamma_c \approx 20$;
3. the origin of S1 is $t_o \approx 1995.7$; and
4. $\chi^2(i_o \approx 6°) \approx 67.4$.

A.2. Determining the family of solutions

The solution is not unique. For the inclination angle previously found, i.e., $i_o \approx 6°$ and using the parameters of the corresponding solution, we gradually varied V_a between $0.01c$ and $0.45c$. At each step of V_a, we minimized the function $\chi^2_t(\lambda)$, where λ are the free parameters. The function $\chi^2(V_a)$ remained constant, indicating a degeneracy of the solution, and we obtained the range of possible values for the precession period given in Table A.1.

Table A.1. Range for the precession period.

V_a	$0.01c$	$0.45c$
$T_p(V_a)$	≈570 000 yr	≈7700 yr

Table A.2. Main solutions found for $i_o \approx 5.98°$.

Solution	$(T_p/T_b)_{min}$	χ^2(min)	Remark
Sol 1	≈3.3	≈50.8	$\gamma_c > 30$
Sol 2	≈11.45	≈53.7	
Sol 3	≈23.0	≈63.9	
Sol 4	≈76	≈63.6	
Sol 5	≈109	≈62.2	$\gamma_c > 30$

A.3. Determining the BBH system parameters

Because the precession is defined by $+\omega_p(t-z/V_a)$, the BBH system rotation is defined by $-\omega_b(t - z/V_a)$. In this section, we kept the inclination angle previously found, i.e., $i_o \approx 6°$ and $V_a = 0.1c$.

To determine the BBH system parameters corresponding to a value of T_p/T_b, we minimized $\chi^2_t(M_1)$ when the mass of the ejecting black hole M_1 varied gradually between 1 $M_\odot$ to a value corresponding to $M_1/M_2 = 2$ with a starting value of M_2, such that $10^6 \leq M_2 \leq 10^9$. During the minimization M_2 is a free parameter, and at each step of M_1, we minimized the function $\chi^2_t(\lambda)$, where λ are the free parameters. Thus we constrained the parameters of the BBH system when the two black holes have the same masses, i.e., $M_1 = M_2$.

We determined the parameters of the BBH system model for different values of the parameter T_p/T_b, namely $T_p/T_b = 4.6$, 10, 22, 46, 100, and 220.

For a given value of T_p/T_b, we found the radius of the BBH system defined by Eq. (8). Note that the radius of the BBH system does not depend on the starting value of M_2.

A.4. $\chi^2(T_p/T_b)$ – diagram

In this section, we kept the inclination angle previously found, i.e., $i_o \approx 6°$, $V_a = 0.1c$ and assumed $M_1 = M_2$.

The diagram $\chi^2(T_p/T_b)$ provides the possible solutions at a given inclination angle. Some of the solutions can be mirage solutions when i_o varies.

We calculated $\chi^2(T_p/T_b)$ for $1 \leq T_p/T_b \leq 300$. We started for each value of the BBH system parameters found in the previous section, i.e., corresponding to the values of $T_p/T_b = 4.6$, 10, 22, 46, 100, and 220, and covered the complete interval $1 \leq T_p/T_b \leq 300$. For instance, if we started at $T_p/T_b = 22$, we covered the ranges varying T_p/T_b from 22 to 1 and from 22 to 300. We found the possible solutions of the BBH system, i.e,. the solutions that correspond to the minima of $\chi^2(T_p/T_b)$. They are given in Table A.2.

Solutions 1 and 5 are excluded because they have $\gamma_c > 30$. There are three possible solutions, the best one is Solution 2, which corresponds to a BBH system whose radius is $R_{bin} \approx 60\ \mu$as. In the following, we continue with Solution 2.

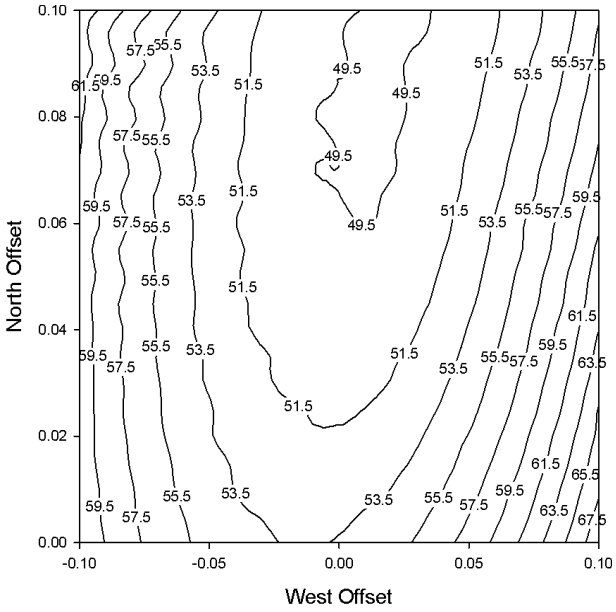

Fig. A.2. Calculation of $\chi^2(\Delta W, \Delta N)$ using the BBH model. Non-zero offsets are possible, but the size of the offset must be the same as the radius of the BBH system calculated at this point. This is the case if the offsets are $\Delta W_1 \approx 0.010$ mas and $\Delta N_1 \approx 0.070$ mas. We determined the offset at $i_o \approx 6°$; it does not depend on the value of the adopted inclination angle.

A.5. Possible offset of the origin of the ejection

In this section, we kept the inclination angle previously adopted, i.e., $i_o \approx 6°$. We assumed that $V_a = 0.1c$, $M_1 = M_2$, $T_p/T_b = 11.45$ and used the parameters of Solution 2 previously found.

To test whether the VLBI component is ejected from the VLBI core or from the second black hole, we calculated $\chi^2(\Delta W, \Delta N)$, where ΔW and ΔN are offsets in the west and north directions. The step used in the west and north directions is 5 μas. At each step of ΔW and ΔN, we minimized the function $\chi^2_t(\lambda)$, where λ are the free parameters (Fig. A.2). The radius of the BBH system was left free to vary during the minimization.

The minimum of $\chi^2(\Delta W, \Delta N)$ is ≈49.5, and we see from Fig. A.2 that the corresponding non-zero offsets are with $\Delta N \geq 0.060$ mas. However, all points with the smallest $\chi^2(\Delta W, \Delta N)$ are not possible. Indeed, for a point with the smallest χ^2, the size of the offset offset must be equal to the radius of the BBH system calculated at this point. This is the case if the offsets are $\Delta W_1 \approx +0.010$ mas and $\Delta N_1 \approx +0.070$ mas. The radius of the BBH system at this point is $R_{bin} \approx 70$ μas and the offset size is ≈71 μas, i.e., the offset and the radius of the BBH system are the same at this point.

Therefore we conclude that

- the VLBI component S1 is not ejected from the VLBI core, but from the second black hole of the BBH system;
- the radius of the BBH system is $R_{bin} \approx 71$ μas. It is about twice the smallest error bars of the observed VLBI component coordinates (the component positions), but it is significantly detected (2σ from Fig. A.2).

We must correct the VLBI coordinates from the offset before we continue.

Note that determining the offset of the origin does not depend on the value adopted for the inclination angle. This was shown by calculating the offset at different inclination angles, i.e., $i_o \approx 4°, 5°, 7°$.

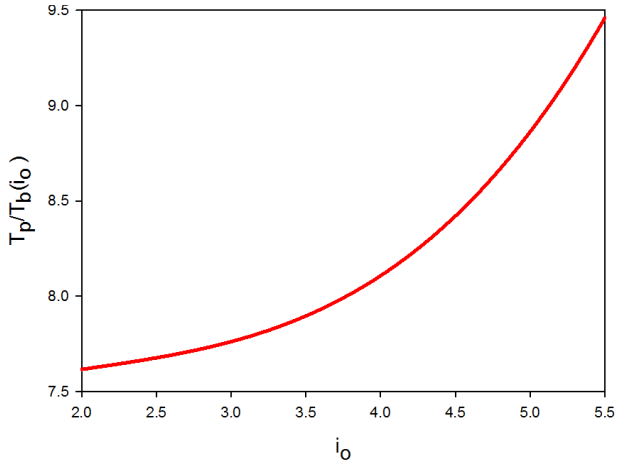

Fig. A.3. T_p/T_b as function of i_o obtained by minimizing $\chi^2(i_o)$.

A.6. Determining T_p/T_b

From this point onward, the original coordinates of the VLBI component S1 are corrected for the offsets ΔW_1 and ΔN_1 found in the previous section. In this section, we assumed that $R_{bin} = 71$ μas, $M_1 = M_2$ and $V_a = 0.1c$.

Previously, we found that Solution 2 is characterized by $T_p/T_b \approx 11.45$ for $i_o \approx 6°$. In this section we obtain the range of possible values of T_p/T_b when i_o varies.

We calculated the funtion $\chi^2(i_o)$ in the inteval $2° \leq i_o \leq 7°$, assuming that the ratio T_p/T_b is free. The relation between T_p/T_b and i_o is plotted in Fig. A.3.

Knowing of the possible values of the ratio T_p/T_b allows us to calculate in the next section the function $\chi^2(i_o)$ for various values of the ratios T_p/T_b and M_1/M_2 and then estimate the mass ratio M_1/M_2 of the BBH system.

A.7. Preliminary determination of i_o, T_p/T_b and M_1/M_2.

In this section, we assumed that $V_a = 0.1c$ and the radius of the BBH system is $R_{bin} = 71$ μas.

We varied i_o between 2 and 7 degrees and calculated $\chi^2(i_o)$ for various values of T_p/T_b and M_1/M_2. The values of T_p/T_b investigated are $T_p/T_b = 11.45$, 8.88, 8.11, 7.76, and 7.62. The values of M_1/M_2 investigated are $M_1/M_2 = 1.0$, 0.5, 0.37, 0.25, and 0.1. For each value of M_1/M_2 we calculated $\chi^2(i_o)$ for all values of T_p/T_b. The plots $\chi^2(i_o)$ for $M_1/M_2 = 1.0$ and 0.37 are shown in Fig. A.4.

The main results are that

- when i_o is larger than about 6 degrees, the bulk Lorentz factor increases and becomes greater than 30, which is excluded;
- the critical value of $M_1/M_2 \approx 0.5$;
- if $M_1/M_2 > 0.5$, the solution $\chi^2(i_o)$ is a mirage solution;
- if $M_1/M_2 < 0.5$, the solution $\chi^2(i_o)$ has a minimum;
- the solutions with a robustness larger than 1.7σ are those with $M_1/M_2 < 0.37$ (see Table B.1);
- when M_1/M_2 decreases, the solutions are more robust, but they are of lower quality, i.e., their χ^2(min) increases (see Table B.1); and
- when $M_1/M_2 < 0.5$, the value of T_p/T_b that produces the best fit is $T_p/T_b \approx 8.88$, independently of the value of M_1/M_2.

We present in Table A.3 the results of solutions corresponding to $T_p/T_b \approx 8.88$ and $M_1/M_2 = 0.1$, 0.25 and 0.37.

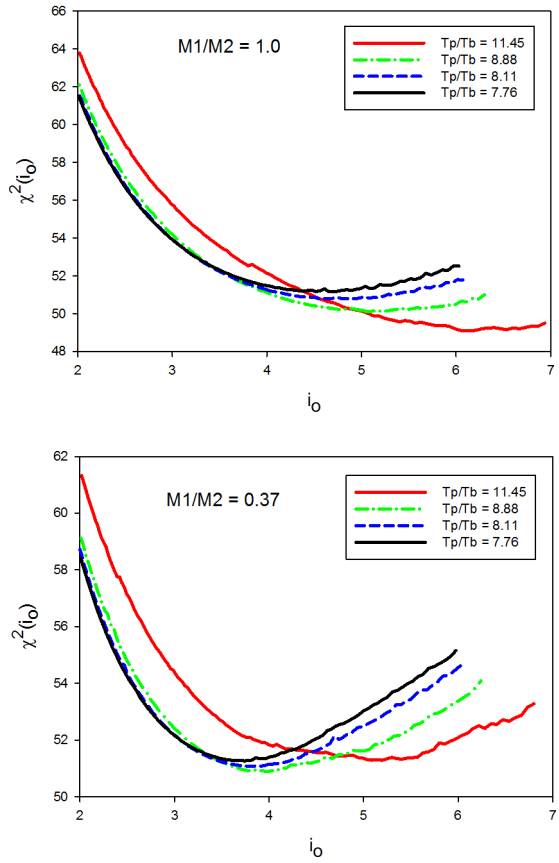

Fig. A.4. Function $\chi^2(i_o)$. It stops at large inclination angles because the bulk Lorentz factor becomes greater than 30. *Top figure*: the ratio M_1/M_2 is $M_1/M_2 = 1$. When T_p/T_b increases, the minimum decreases and disappears. This means that the function $\chi^2(i_o)$ does not show a minimum and is a mirage solution. *Bottom figure*: the ratio $M_1/M_2 = 0.37$. The function $\chi^2(i_o)$ has a minimum for $T_p/T_b \approx 8.88$ and $i_o \approx 4$. The robustness of this solution, defined as the square root of the difference $\chi^2(\gamma = 30) - \chi^2(\min)$, is $\approx 1.8 \times \sigma$.

Table A.3. Solutions found for $T_p/T_b \approx 8.88$.

M_1/M_2	0.1	0.25	0.37
i_o	$\approx 4.10°$	$\approx 3.64°$	$\approx 3.98°$
$\chi^2(\min)$	≈ 53.7	≈ 51.5	≈ 50.9
Robustness(i_o)	$\approx 2.4\sigma$	$\approx 1.9\sigma$	$\approx 1.8\sigma$

A.8. Determining a possible new offset correction

In this section, we assumed $V_a = 0.1c$. Using the solution found in the previous section (Table B.1), we can verify whether if there is an additional correction to the offset of the origin of the VLBI component. For this, we calculated $\chi^2(\Delta W, \Delta N)$, where ΔW and ΔN are offsets in the west and north directions. We assumed the radius of the BBH system to be free to vary. We found that a small additional correction is needed $\Delta W_2 \approx -0.005$ mas and $\Delta N_2 \approx -0.010$ mas.

Finally, we found that the total offset is ≈ 60 μas and the radius of the BBH system is also $R_{bin} \approx 60$ μas.

A.9. Final fit of component S1 of 1823+568

From this point onward, the coordinates of the VLBI component S1 are corrected for the new offsets ΔW_2 and ΔN_2 found in the previous section. In this section, we assumed $V_a = 0.1c$ and $R_{bin} = 60$ μas.

Table A.4. The range of M_1/M_2 when $T_p/T_b \approx 8.88$.

M_1/M_2	0.09	0.17	0.29
i_o	$\approx 3.79°$	$\approx 3.98°$	$\approx 4.27°$
$\chi^2(\min)$	≈ 51.7	≈ 51.2	≈ 50.7
Robustness(i_o)	$\approx 2.4\sigma$	$\approx 2.2\sigma$	$\approx 1.8\sigma$

Table A.5. The range of M_1/M_2 when $T_p/T_b \approx 9.88$.

M_1/M_2	0.095	0.16	0.25
i_o	$\approx 4.06°$	$\approx 4.22°$	$\approx 4.53°$
$\chi^2(\min)$	≈ 51.7	≈ 51.2	≈ 50.7
Robustness(i_o)	$\approx 2.2\sigma$	$\approx 1.8\sigma$	$\approx 1.7\sigma$

We can now find the final solution for S1. We calculated $\chi^2(i_o)$ for various values of T_p/T_b assuming $M_1/M_2 \approx 0.25$. We found that the best range for T_p/T_b is: $8.88 \leq T_p/T_b \leq 9.88$. With this we can estimate the range of the mass ratio assuming $T_p/T_b \approx 8.88$ and $T_p/T_b \approx 9.88$. We defined the range of the mass ratio in the following way:

1. we found the mass ratio that produces a solution of at least 1.7σ robustness, and
2. we found the mass ratio that produces a solution that is poorer by 1σ than the previous one, but that is more robust.

The results of the fit are presented in Tables A.4 and A.5. The improvement of the solutions of Tables A.4 and A.5 compared to the solutions of Table A.3 is due to the new offset and the new value of the BBH system radius.

We see that the solutions found with $T_p/T_b \approx 8.88$ are slightly more robust, but both solutions can be used.

The characteristics of the final solution of the BBH system associated with 1823+568 are given in Sect. 4.4.

Appendix B: Fit of component C5 of 3C 279

B.1. Fit of C5 using the precession model

To fit the ejection of component C5 we used 152 observations (76 epochs).

We studied the two cases $\pm\omega_p(t - z/V_a)$. The final solution of the fit of component C5 of 3C 279 using a BBH system corresponds to $-\omega_p(t - z/V_a)$, therefore we discuss only this case in this appendix.

To fit the component C5, we assumed $T_d \leq 2000$ yr.

In this section, we assume that $V_a = 0.1c$.

The range of inclination explored is $0.5° \leq i_o \leq 10°$.

To begin, we allowed the time origin of the VLBI component to be a free parameter. We assumed $1997.0 \leq t_o \leq 1998.5$. We found that the function $\chi^2_t(i_o)$ is characteristic of a function corresponding to case II (see Sect. 5.1), and the possible range for the inclination angle is [0.5, 5.5]. The time origin is $t_o \approx 1997.52$ when $i_o \to 0.55$, and the time origin is $t_o \approx 1998.15$ when $i_o \to 5.5$. We plotted the first peak flux corresponding to the solution $t_o \approx 1998.15$ and $i_o \to 5.5$ (solution with the smallest χ^2) and found that it is too early by at least eight months (dash line in Fig. B.2). As indicated in Sect. A.1, we do not aim to fit the flux light curve, but we wish to compare the time position of the modeled first peak flux with the observed first peak flux (Fig. B.2).

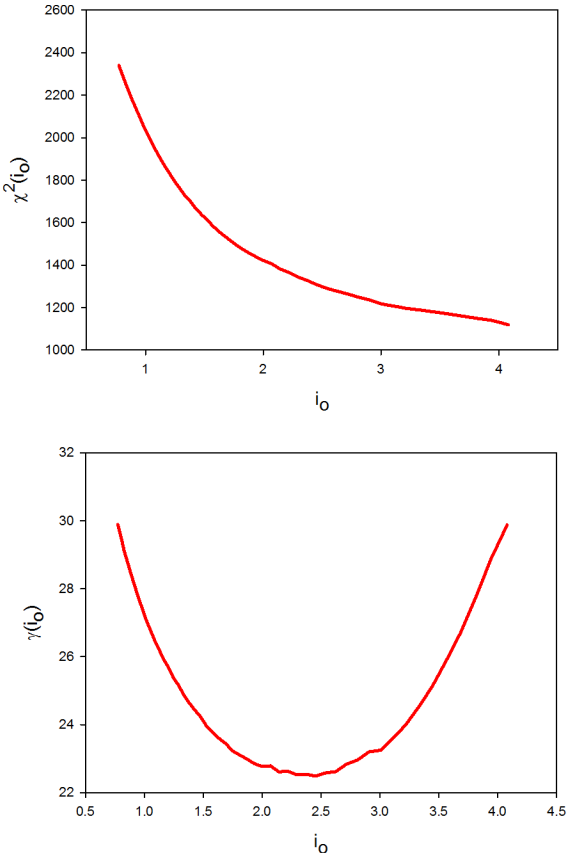

Fig. B.1. Precession model applied to the component C5 of 3C 279. We assumed that the time origin is $1998.80 \leq t_o \leq 1999.10$. *Top figure*: the function $\chi^2(i_o)$ is limited to $0.8° \leq i_o \leq 4.3°$ and has no minimum in this interval. It stops at $i_o \approx 4.3°$ and $i_o \approx 0.8°$ because at these points the bulk Lorentz factor becomes larger than 30. *Bottom figure*: the bulk Lorentz factor diverges when $i_o \to 4.3°$ and $i_o \to 0.8°$.

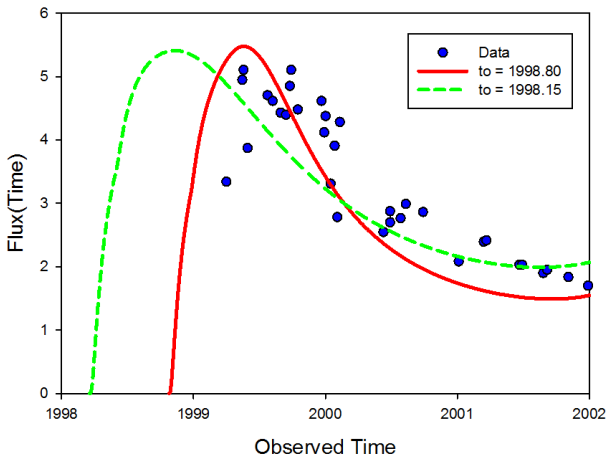

Fig. B.2. Determination of the minimum time for the ejection of component C5. We fit the first peak flux of component C5 of 3C 279 using the precession model. The peak flux corresponding to an ejection at $t_o \approx 1998.15$ is shown (dash line), it is too early by at least 8 months. The precession model can fit the position of the first peak flux for $t_o \geq 1998.80$ (solid line).

Table B.1. Range for the precession period.

V_a	$0.01c$	$0.45c$
$T_p(V_a)$	≈91 900 yr	≈1150 yr

Next, we allowed t_o to be a free parameter in the range $1998.80 \leq t_o \leq 1999.10$ and calculated the new function $\chi^2_t(i_o)$. The possible range for the inclination angle is reduced to $0.8° \leq i_o \leq 4.3°$. The plots of $\chi^2_t(i_o)$ and $\gamma(i_o)$ are presented in Fig. B.1. We plotted the first peak flux corresponding to the solution $t_o \approx 1998.80$ and $i_o \to 4.3$ (solid line in Fig. B.2). From Fig. B.2, we conclude that the minimun time for the ejection of C5 is $t_o \geq 1998.80$.

The behavior of the functions $\chi^2(i_o)$ and $\gamma_c(i_o)$ are the second signature of case II, i.e., the offset is larger than the smallest error bars of the VLBI component coordinates.

We see from Fig. B.1 that the bulk Lorentz factor is $\gamma_c \geq 22$. Because the function $\chi^2(i_o)$ does not show a minimum, we arbitrarily chose an inclination angle such that $22 \leq \gamma \leq 26$ and the corresponding $\chi^2(i_o)$ is the smallest. To continue, we chose $i_o \approx 2.98°$ and the corresponding parameters of the precession solution (the χ^2 of this solution is $\chi^2 \approx 1211$ and its bulk Lorentz factor is $\gamma \approx 22.6$). We used this solution to apply the method explained in Sect. 3 and we will see in the following how the BBH system model allows us to find the concave part of the funtion $\chi^2(i_o)$.

B.2. Determining the family of solutions (precession model)

The solution is not unique. For the inclination angle previously found, i.e., $i_o \approx 2.98°$ and using the parameters of the corresponding solution, we gradually varied V_a between $0.01c$ and $0.45c$. The function $\chi^2(V_a)$ remains constant, indicating a degeneracy of the solution, and we obtained the range of possible values for the precession period given in Table B.1.

B.3. Possible offset of the origin of the ejection (precession model)

In this section, we kept the inclination angle previously found, i.e., $i_o \approx 2.98°$. We assumed that $V_a = 0.1$ and used the parameters of the solution previously found.

To test whether the VLBI component is ejected from the VLBI core or if it is ejected with an offset of the origin, we calculated $\chi^2(\Delta W, \Delta N)$, where ΔW and ΔN are offsets in the west and north directions, using the precession model. The step used in West and North directions is 10 μas.

We see from Fig. B.3, that non-zero offsets are possible and the smallest offsets of the coordinates are $\Delta W \approx +0.300$ mas and $\Delta N \approx +0.280$ mas, which, a priori, corresponds to an offset of the space origin of ≥410 μas or to a BBH system of radius $R_{bin} \geq 410\,\mu$as. This minimum offset corresponds to an improvement of about 28σ. If the offset of the space origin can be estimated using the precession model, it cannot be explained if we assume that the nucleus contains a single black hole, but it can be explained if we assume that the nucleus contains a BBH system.

It is important to note that the offset does not depend on the inclination angle chosen in Sect. B.1. Indeed, we took the solution corresponding to $i_o \approx 1.5°$, whose χ^2 is $\chi^2 \approx 1610$ and whose bulk Lorentz factor is $\gamma \approx 24$, and we calculated $\chi^2(\Delta W, \Delta N)$, which yielded the same result.

It is easy to prove that the value of the offset of the space origin is related to the time origin problem. Indeed, Fig. B.3 shows that there is a significant offset of the space origin when we assume that the time origin of component C5 of 3C 279 is $t_o \geq 1998.80$. Now, using again the precession model, we

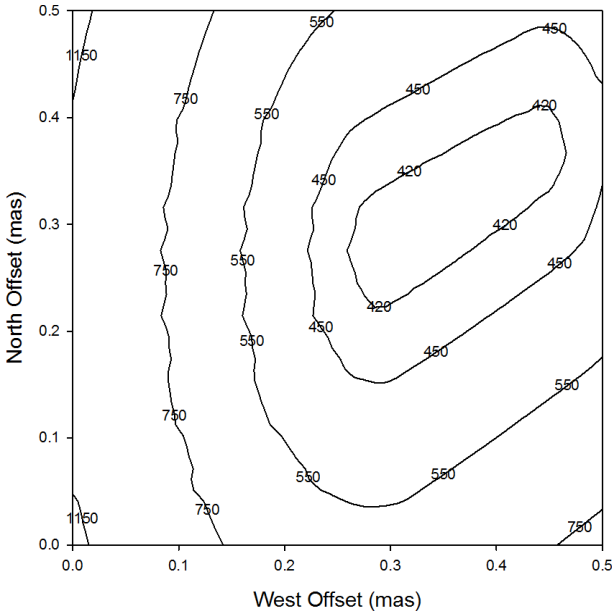

Fig. B.3. Using the precession model, we calcuated $\chi^2(\Delta W, \Delta N)$ corresponding to the solution with $i_o \approx 2.98°$. Non-zero offsets are possible and the smallest offsets are $\Delta W \approx 0.300$ mas and $\Delta N \approx 0.280$ mas, which corresponds to a BBH system of radius $R_{bin} \geq 410\ \mu$as.

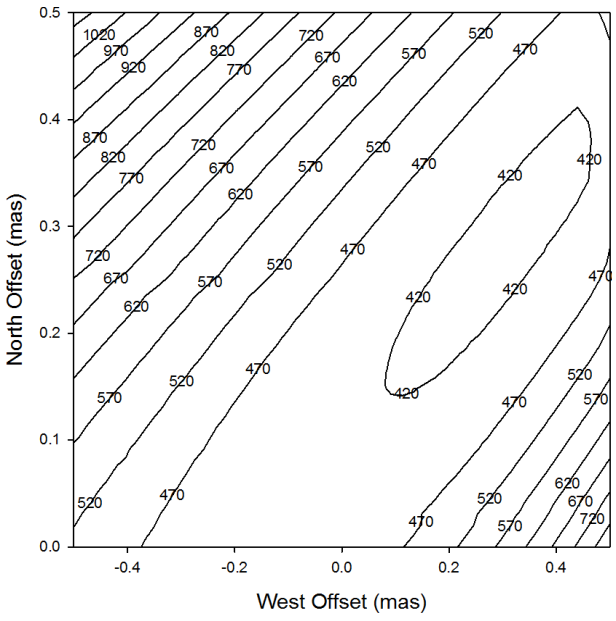

Fig. B.4. Calculation of $\chi^2(\Delta W, \Delta N)$ using the precession model and assuming that the time origin is a free parameter. We find that non-offset are possible and the smallest offset corresponds to the point $\Delta W \approx 100\ \mu$as and $\Delta N \approx +150\ \mu$as. At this point, the time origin is $t_o \approx 1998.45$ which is ≈7 months too early.

calculated the possible offset of the space origin assuming that the time origin is a free parameter (Fig. B.4). We see from Fig. B.4 that non-zero offsets are possible and the smallest offsets of the coordinates are $\Delta W \approx 100\ \mu$as and $\Delta N \approx +150\ \mu$as, at this point, the time origin is $t_o \approx 1998.45$. This time origin corresponds to an ejection that is about seven months too early.

To continue, two possibilities arise:

1. either we keep the original VLBI coordinates and determine the parameters of the BBH system and the $\chi^2(T_p/T_b)$ – diagram. Then, we determine a first offset correction using the BBH model, and after a preliminary determination of T_p/T_b and M_1/M_2, we determine a second offset correction using the BBH model;
2. or we apply the precession offset correction to the VLBI coordinates and then we determine the parameters of the BBH system and the $\chi^2(T_p/T_b)$ – diagram. Then we determine a first offset correction using the BBH model, and after a preliminary determination of T_p/T_b and M_1/M_2, we determine a second offset correction using the BBH model.

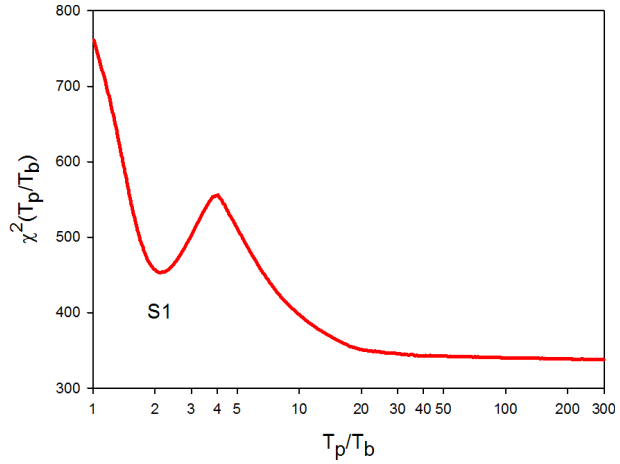

Fig. B.5. Calculation of $\chi^2(T_p/T_b)$. The curve corresponds to the minimization when T_p/T_b varies from 1 to 300. There is one solution S1.

For component C5 of 3C 279, the two possibilities were followed. We found that they provide the same result in the end. In this article, we present the first one.

The determination of the offsets of the origin of the ejection does not depend on the inclination angle.

B.4. Determining the BBH system parameters

Because the precession is defined by $-\omega_p(t - z/V_a)$, the BBH system rotation is defined by $+\omega_b(t - z/V_a)$. In this section we kept the inclination angle previously found, i.e., $i_o \approx 2.98°$ and $V_a = 0.1c$.

In the previous section, we saw that the BBH system has a large radius, i.e., $R_{bin} \geq 410\ \mu$as. Therefore, we determined the parameters of a BBH system with small T_p/T_b and a radius for the BBH system that is a free parameter (solutions with small T_p/T_b have large radii), i.e., we determined the parameters of a BBH system with $T_p/T_b = 1.01$ and calculated the corresponding $\chi^2(T_p/T_b)$ – diagram.

B.5. $\chi^2(T_p/T_b)$ – diagram

In this section, we kept the inclination angle previously found, i.e., $i_o \approx 2.98°$, $V_a = 0.1c$ and assumed $M_1 = M_2$. Furthermore we assumed that the radius of the BBH system is a free parameter.

We calculated $\chi^2(T_p/T_b)$ for $1 \leq T_p/T_b \leq 300$. We started for BBH system parameters corresponding to the values of $T_p/T_b = 1.01$ and cover the complete interval of T_p/T_b. The result is shown in Fig. B.5.

We found the one solution given in Table B.2.

Table B.2. Solution found for $i_o \approx 2.98°$.

Solution	$(T_p/T_b)_{min}$	χ^2(min)	R_{bin}
S1	≈2.13	≈453	≈389 μas

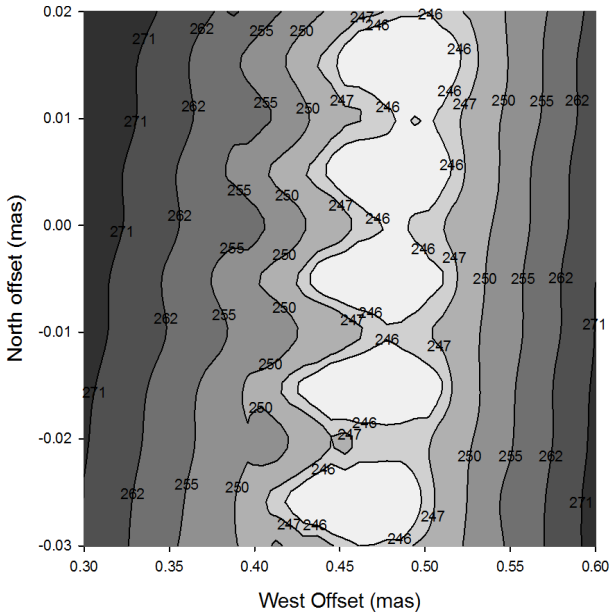

Fig. B.6. Calculation of $\chi^2(\Delta W, \Delta N)$ using the BBH model. Contour levels are 246, 247, 250, 255, etc., corresponding to the minimum, 1σ, 2σ, 3σ, etc. There is a valley of possible offsets, but the size of the offset must be the same as the radius of the BBH system. This is true when the offsets are $\Delta W_1 \approx +0.490$ mas and $\Delta N_1 \approx 0.005$ mas.

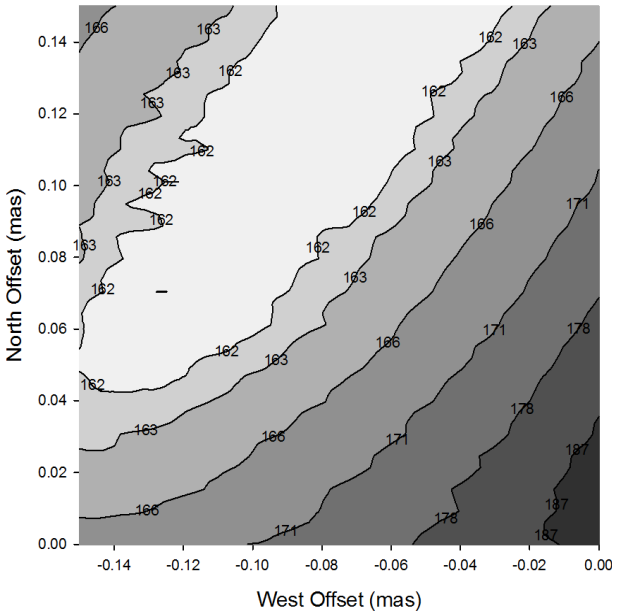

Fig. B.7. Calculation of $\chi^2(\Delta W, \Delta N)$ using the BBH model. Contour levels are 162, 163, 166, 171, etc corresponding to the minimum, 1σ, 2σ, 3σ, etc. There is a valley of possible offsets, but the size of the offset must be the same as the radius of the BBH system. This is the case when the offsets are $\Delta W_2 \approx -0.085$ mas and $\Delta N_2 \approx +0.105$ mas.

B.6. Determining the offset of the origin of the ejection (BBH model)

In this section, we kept the inclination angle previously found, i.e., $i_o \approx 2.98°$. We assumed that $V_a = 0.1c$, $M_1 = M_2$.

We calculated $\chi^2(\Delta W, \Delta N)$, where ΔW and ΔN are offsets in the west and north directions. The step used in the west and north directions is 5 μas. The radius of the BBH system and T_p/T_b are free parameters during the minimization.

We calculated $\chi^2(\Delta W, \Delta N)$ starting with the parameters of solution S1 found in the previous section. The result is shown in Fig. B.6.

We see from Fig. B.6 that non-zero offsets are possible. However, all points with the smallest $\chi^2(\Delta W, \Delta N)$ are not possible. Indeed, for a point with the smallest χ^2, the offset size must be equal to the radius of the BBH system calculated at this point. This is the case if the offsets are $\Delta W_1 \approx +0.490$ mas and $\Delta N_1 \approx +0.005$ mas.

The radius of the BBH system at this point is $R_{bin} \approx 487$ μas and the offset size is ≈490 μas, i.e., the offset and the radius of the BBH system are the same at this point.

Therefore we conclude that

- the VLBI component C5 is not ejected from the VLBI core, but from the second black hole of the BBH system, and
- the radius of the BBH system is $R_{bin} \approx 490$ μas. It is more than ten times the smallest error bars of the VLBI component coordinates.

Note that if the size of the offset found with the BBH model is the same as the size of the offset found with the precession model, the first offsets are not the same for the coordinates. However, after the preliminary determination of the ratios T_p/T_b and M_1/M_2, the second and third offset corrections provide the same final offset corrections (the two methods indicated in Sect. B.3 provide the same corrections in the end).

B.7. Preliminary determination of i_o, T_p/T_b and M_1/M_2

From this point onward, the original coordinates of the VLBI component C5 are corrected for the offsets ΔW_1 and ΔN_1 found in the previous section. In this section, we assumed that $V_a = 0.1c$ and the radius of the BBH system is $R_{bin} = 490$ μas.

For given values of the ratio $M_1/M_2 = 1.0$, 1.25, 1.50, 1.75, and 2.0, we varied i_o between 3.0 and 10 degrees and calculated $\chi^2(i_o)$ assuming that the ratio T_p/T_b is variable.

We found that $\chi^2(i_o)$ is minimum for the parameters

- $i_o \approx 5.9°$;
- $M_1/M_2 \approx 1.75$; and
- $T_p/T_b \approx 14.6$.

B.8. Detemining a possible new offset correction

In this section, we assumed $V_a = 0.1c$.

With $i_o \approx 5.9°$, with a variable ratio T_p/T_b, $M_1/M_2 \approx 1.75$ and the parameters of the solution found in the previous section, we can verify whether there is an additional correction to the offset of the origin of the VLBI component. We calculated $\chi^2(\Delta W, \Delta N)$, where ΔW and ΔN are offsets in the west and north directions. We assumed that the radius of the BBH system is left free to vary. The result is shown in Fig. B.7. We found that an additional correction is needed, namely $\Delta W_2 \approx -0.085$ mas and $\Delta N_2 \approx +0.105$ mas.

At this point the total offset is ≈418 μas and the radius of the BBH system is $R_{bin} \approx 420$ μas.

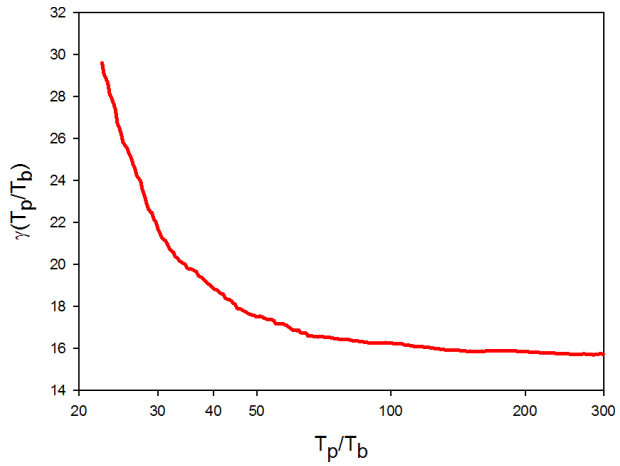

Fig. B.8. Calculation of $\gamma(T_p/T_b)$. For a given value of M_1/M_2, the bulk Lorentz factor decreases when T_p/T_b increases, showing that if the ratio T_p/T_b is high enough, we can find solutions that are not mirage solutions in relation to the variable γ.

Table B.3. Solutions found for $T_p/T_b = 140$.

M_1/M_2	2.50	2.75	3.00
i_o	≈10.0°	≈10.4°	≈11.2°
χ^2(min)	≈151.7	≈151.4	≈152.0
γ_{min}	≈15.0	≈16.7	≈21.4

B.9. Final fit of component C5 of 3C 279

The coordinates of the VLBI component C5 are corrected for the new offsets ΔW_2 and ΔN_2. In this section, we assumed $V_a = 0.1c$ and $R_{bin} = 420\ \mu$as.

We can now find the final solution for the fit of C5. We calculated $\chi^2(i_o)$ for various values of T_p/T_b and M_1/M_2, namely $T_p/T_b \leq 1000$ and $M_1/M_2 \leq 3.5$ with a typical step $\Delta(M_1/M_2) = 0.25$.

The first important result is that when the ratio T_p/T_b is high enough, we can find non-mirage solutions in relation to the variable γ. To illustrate this result, we plot in Fig. B.8 the function $\gamma(T_p/T_b)$ corresponding to $M_1/M_2 = 1.75$.

The determination of the solution used an iterative method. Starting with a given value of T_p/T_b, we calculated $\chi^2(i_o)$ for various values of M_1/M_2. Then we calculated for the parameters corresponding to the solution found the function $\chi^2(T_p/T_b)$ to determine the new value of T_p/T_b that minimizes the function $\chi^2(T_p/T_b)$. Starting with the new value of T_p/T_b, we repeated the procedure.

At each step of the procedure, we calculated $\chi^2(\gamma)$ to check that the solution corresponds to the concave part and is not a mirage solution.

The best fit is obtained for $T_p/T_b \approx 140$ and $M_1/M_2 \approx 2.75$. The results of the fits are presented in Table B.3.

We plot in Fig. B.9 the calculation of $\chi^2(\gamma)$ corresponding to the solution characterized by $T_p/T_b = 140$ and $M_1/M_2 = 2.75$. It shows that the solution is not a mirage solution in relation to γ.

The best fit is obtained for $T_p/T_b \approx 140$ (see Fig. B.10). When the ratio T_p/T_b increases, the χ^2 remains mostly constant but the robustness of the solution in relation to γ increases.

Finally, we plot in Fig. B.11 the function $\chi^2(i_o)$.

The characteristics of final solution of the BBH system associated with 3C 279 are given in Sect. 5.4.

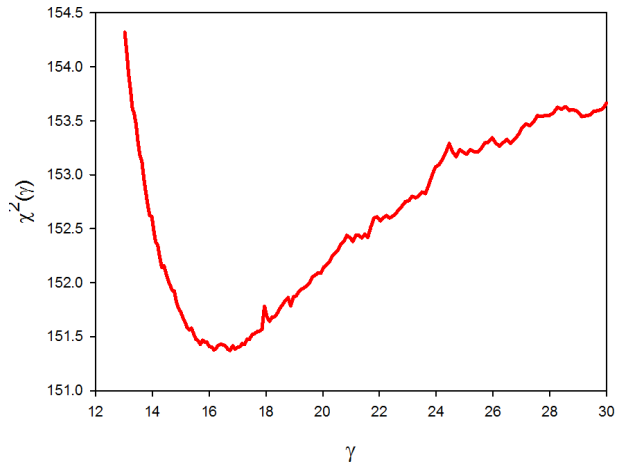

Fig. B.9. Calculation of $\chi^2(\gamma)$ for the solution with $T_p/T_b = 140$ and $M_1/M_2 = 2.75$. It shows that the solution is not a mirage solution in relation to γ. The minimum corresponds to $\gamma \approx 16.7$.

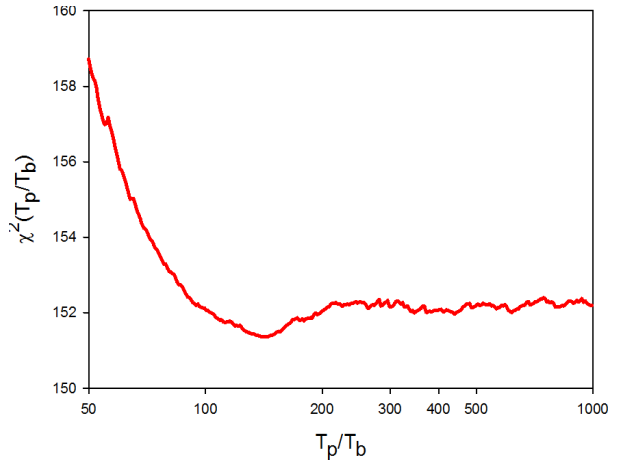

Fig. B.10. Calculation of $\chi^2(T_p/T_b)$ for the solution with $M_1/M_2 = 2.7$

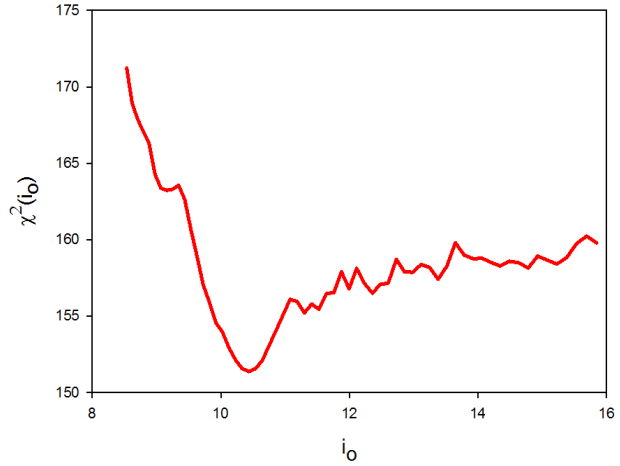

Fig. B.11. Calculation of $\chi^2(i_o)$ for the solution with $T_p/T_b = 140$ and $M_1/M_2 = 2.75$.

Appendix C: Error bars

C.1. Minimum error bar values

Observations used to fit the components S1 of 1823+568 and C5 of 3C 279 were performed at 15 GHz. We adopted for the

minimum values of the error bars, $\Delta_{\rm min}$, values in the range $Beam/15 \leq \Delta_{\rm min} \leq Beam/12$.

There are three important points concerning the minimum values used for the error bars:

1. The minimum values are chosen empirically, but the adopted values are justified a posteriori by comparing of the value of χ^2 of the final solution and the number of constraints used to make the fit. Indeed, the reduced χ^2 has to be close to 1.
2. The minimum value of the error bars used at 15 GHz produces a value of $(\chi^2)_{\rm final}$ concistent with the value of the realistic error obtained from the VLBI Service for Geodesy and Astrometry (Schlüter & Behrend 2007), which is a permanent geodetic and astrometric VLBI program. It has been monitoring the position of thousands of extragalactic radio sources for more than 30 years. In 2009, the second realization of the International Celestial Reference Frame (ICRF2) was released (Fey et al. 2009), obtained after the treatment of about 6.5 millions of ionosphere-corrected VLBI group delay measurements at 2 and 8 GHz. This catalog is currently the most accurate astrometric catalog, giving absolute positions of 3414 extragalactic bodies at 8 GHz. The observations at 2 GHz are used for the ionospheric correction only. Therefore, the positions at 2 GHz are not provided. The ICFR2 is found to have a noise floor of only 40 microseconds of arc (μas), which is five to six times better than the previous ICRF realization (Ma et al. 1998). The positions of more than 200 radio sources are known with a precision (inflated error, or "realistic" error) better than 0.1 mas.
   Since the ICRF2 release, the positional accuracy of the sources has increased, and it is likely that the next VLBI realization of the ICRF will have a noise floor lower than 40 μas.
3. The adopted minimum value of the error bars also includes typical errors due to opacity effects, which shift the measured position at different frequencies (Lobanov 1998).

Thus the minimum values for the error bars adopted at 15 GHz, using Eq. (19), are correct. The fit of VLBI coordinates of components of 3C 345 (work in progress) indicates that the adopted values for the minimun values of the error bars, using Eq. (19), are correct for frequencies between 8 GHz and 22 GHz. At lower frequencies, the minimum values may be higher than $Beam/12$ due to strong opacity effects and at 43 GHz, the minimum values are also probably higher ($\approx$20 μas).

It has been suggested by Lister & Homan (2005) that the positional error bars should be about 1/5 of the beam size. To study the influence of the minimum values of the error bars on the characteristics of the solution, we calculate in the next sections the solution of the fit of the component C5 assuming for the minimum values of the error bars the value suggested by Lister & Homan (2005), i.e. the value $\Delta_{\rm min} = Beam/5$, or $(\Delta W)_{\rm min} \approx 102$ μas and $(\Delta N)_{\rm min} \approx 267$ μas.

C.2. Fit of C5 using the precession model

We look for a solution with $-\omega_{\rm p}(t - z/V_a)$ and $t_{\rm o} \geq 1980.80$ (see Sect. B.1).

In this section, we assumed that $V_a = 0.1c$.

The range of inclination explored is $0.5° \leq i_{\rm o} \leq 10°$.

We allowed $t_{\rm o}$ to be a free parameter in the range $1998.80 \leq t_{\rm o} \leq 1999.10$ and calculated the function $\chi^2_t(i_{\rm o})$. The possible range for the inclination angle is $0.74° \leq i_{\rm o} \leq 4.3°$. The plots of $\chi^2_t(i_{\rm o})$ and $\gamma(i_{\rm o})$ are presented in Fig. C.1.

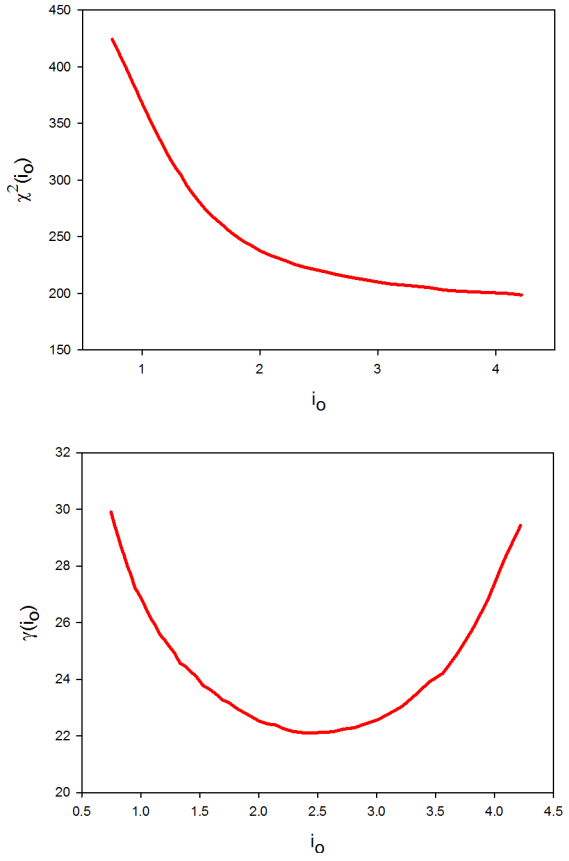

Fig. C.1. Precession model applied to the component C5 of 3C 279 assuming high values for the minimum error bars. We assumed that the time origin is $1998.80 \leq t_{\rm o} \leq 1999.10$. *Top figure*: the function $\chi^2(i_{\rm o})$ is limited to $0.8° \leq i_{\rm o} \leq 4.3°$ and has no minimum in this interval. It stops at $i_{\rm o} \approx 4.3°$ and $i_{\rm o} \approx 0.8°$ because at these points the bulk Lorentz factor becomes larger than 30. *Bottom figure*: the bulk Lorentz factor diverges when $i_{\rm o} \rightarrow 4.3°$ and $i_{\rm o} \rightarrow 0.8°$.

The behavior of the functions $\chi^2(i_{\rm o})$ and $\gamma_{\rm c}(i_{\rm o})$ are the second signature of case II.

Comparison of Figs. C.1 and B.1 shows that the range of the inclination angle, and the values of the bulk Lorentz factor in this range, are the same for the different values of the minimum error bars used.

C.3. Possible offset of the origin of the ejection (precession model)

In this section, we kept the inclination angle used in Sect. B.3, i.e., $i_{\rm o} \approx 3.3°$. We assumed that $V_a = 0.1$ and used the parameters of the solution found in Sect. C.2.

We calculated $\chi^2(\Delta W, \Delta N)$, where ΔW and ΔN are offsets in the west and north directions, using the precession model. The step used in the west and north directions is 10 μas. The result of the calculation is plotted in Fig. C.2.

Comparison of Fig. C.2 with Fig. B.3 shows that

- the smallest offsets of the coordinates are $\Delta W \approx +0.320$ mas and $\Delta N \approx +0.280$ mas. They are similar to the offsets found assuming that the minimum error bars are $\Delta_{\rm min} = Beam/15$ (see Sect. B.3),
- the value of χ^2 at the minimum is $\chi^2_{\rm min} \approx 67$ instead of $\chi^2_{\rm min} \approx 400$ when the minimum error bars are $\Delta_{\rm min} = Beam/15$. The reduced $\chi^2_{\rm r}$ is $\chi^2_{\rm r} \approx 67/152 \approx 0.44$, indicating that the minimum error bars are too large.

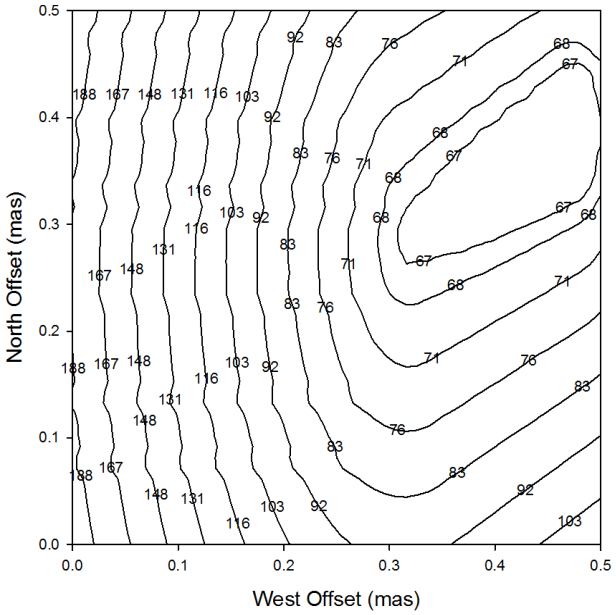

Fig. C.2. Using the precession model, we calcuated $\chi^2(\Delta W, \Delta N)$. The contour levels 68, 71, 76, etc correspond to 1σ, 2σ, 3σ, etc. Non-zero offsets are possible and the smallest offsets are $\Delta W \approx 0.320$ mas and $\Delta N \approx 0.280$ mas, which corresponds to a BBH system of radius $R_{\rm bin} \geq 425$ μas.

Table C.1. Solution found for $i_{\rm o} \approx 2.98°$.

Solution	$(T_{\rm p}/T_{\rm b})_{\rm min}$	χ^2(min)	$R_{\rm bin}$
Sol 1	≈2.24	≈64.6	≈398 μas

Accordingly, with high values for the minimum values of the error bars, we find using the precession model that the component C5 is ejected with an offset of the space origin of at least 0.425 mas with a robustness higher than 11σ. The offset of the space origin can be estimated using a single black hole and the precession of the accretion disk. It cannot be explained when we assume that the nucleus contains a single black hole, but it can be explained when we assume that the nucleus contains a BBH system.

C.4. $\chi^2(T_{\rm p}/T_{\rm b})$ – diagram

Because the precession is defined by $-\omega_{\rm p}(t-z/V_a)$, the BBH system rotation is defined by $+\omega_{\rm b}(t-z/V_a)$. As in Sect. B.4, we calculated the BBH parameters for the inclination angle $i_{\rm o} \approx 2.98°$ and the ratio $T_{\rm p}/T_{\rm b} = 1.01$ and calculated the corresponding $\chi^2(T_{\rm p}/T_{\rm b})$ – diagram assuming $M_1 = M_2$ and $V_a = 0.1c$.

We calculated $\chi^2(T_{\rm p}/T_{\rm b})$ for $1 \leq T_{\rm p}/T_{\rm b} \leq 300$. The result is shown in Fig. C.3.

We found a possible solution of the BBH system given in Table C.1.

Comparison of Tables B.2 and C.1 and of Figs. B.5 and C.3 shows that the solutions S1 and Sol1 are mostly identical.

C.5. Determining the offset of the origin of the ejection (BBH model)

In this section, we kept the inclination angle previously found, i.e., $i_{\rm o} \approx 2.98°$. We assumed that $V_a = 0.1c$, $M_1 = M_2$.

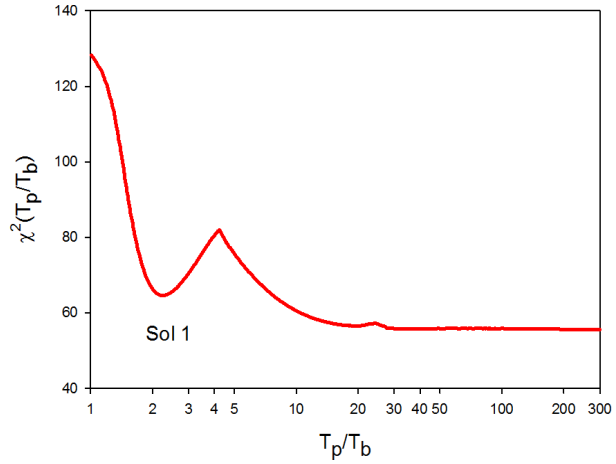

Fig. C.3. Calculation of $\chi^2(T_{\rm p}/T_{\rm b})$. There is one solution Sol 1.

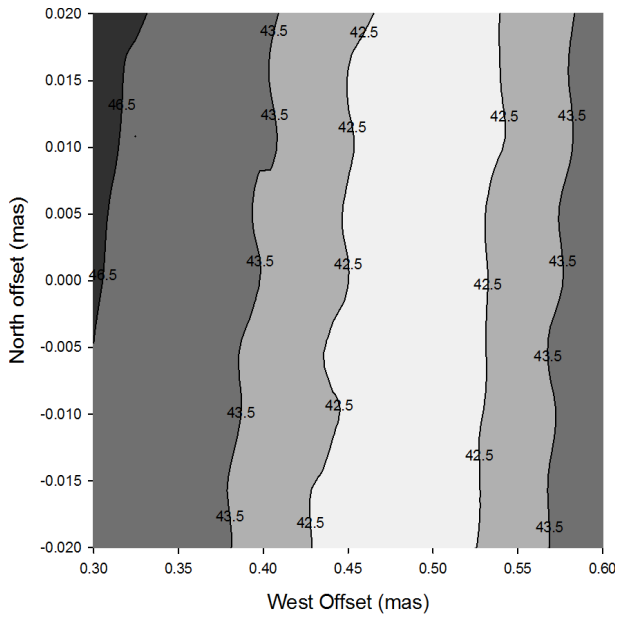

Fig. C.4. Calculation of $\chi^2(\Delta W, \Delta N)$ using the BBH model. There is a valley of possible offsets, but the size of the offset must be the same as the radius of the BBH system. This is the case if the offsets are $\Delta W_1 \approx +0.495$ mas and $\Delta N_1 \approx 0.005$ mas. The corresponding radius of the BBH system is $R_{\rm bin} \approx 495$ μas.

We calculated $\chi^2(\Delta W, \Delta N)$, where ΔW and ΔN are offsets in the west and north directions. The step used in the west and north directions is 5 μas. The radius of the BBH system and $T_{\rm p}/T_{\rm b}$ are free parameters during the minimization.

We calculated $\chi^2(\Delta W, \Delta N)$ starting with the parameters of solution Sol 1 found in the previous section. The result is shown in Fig. C.4.

We see from Fig. C.4 that non-zero offsets are possible. However, all points with the smallest $\chi^2(\Delta W, \Delta N)$ are not possible. Indeed, for a point with the smallest χ^2, the size offset must be equal to the radius of the BBH system calculated at this point. This is the case if the offsets are $\Delta W_1 \approx +0.495$ mas and $\Delta N_1 \approx +0.005$ mas.

The radius of the BBH system at this point is $R_{\rm bin} \approx 495$ μas and the offset size is ≈495 μas, i.e. the offset and the radius of the BBH system are the same at this point.

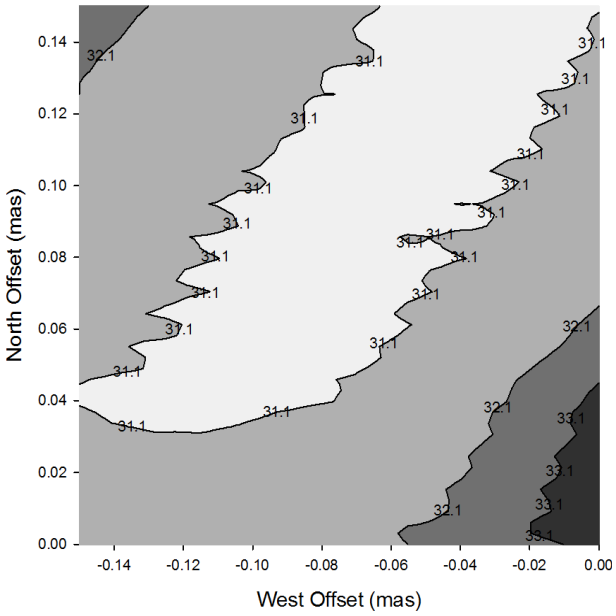

Fig. C.5. Calculation of $\chi^2(\Delta W, \Delta N)$ using the BBH model. There is a valley of possible offsets, but the size of the offset must be the same as the radius of the BBH system. This is the case if the offsets are $\Delta W_2 \approx -0.085$ mas and $\Delta N_2 \approx 0.085$ mas. The corresponding radius of the BBH system is $R_{\rm bin} \approx 419$ μas.

Comparison of the result found in Sect. B.6 and of Figs. C.4 and B.6 show that the offset determined using large error bars is the same as the offset calculated with the small error bars.

Therefore we conclude that the VLBI component C5 is not ejected from the VLBI core but from the second black hole of the BBH system.

C.6. Determining a possible new offset correction

From this point onward, the original coordinates of the VLBI component C5 are corrected for the offsets ΔW_1 and ΔN_1 found in the previous section.

In this section, we assumed $V_a = 0.1c$.

As in Sect. B.7, we preliminarily determined the parameters $T_{\rm p}/T_{\rm b}$, M_1/M_2 and $i_{\rm o}$.

With $i_{\rm o} \approx 5.9°$, using the ratios $T_{\rm p}/T_{\rm b}$ free and $M_1/M_2 \approx 1.75$, we can verify whether there is an additional correction to the offset of the origin of the VLBI component. We calculated $\chi^2(\Delta W, \Delta N)$, where ΔW and ΔN are offsets in the west and north directions. We assumed that the radius of the BBH system is let free to vary. The result is shown in Fig. C.5. We found that an additional correction is needed, namely $\Delta W_2 \approx -0.085$ mas and $\Delta N_2 \approx +0.085$ mas.

At this point the total offset is ≈419 μas and the radius of the BBH system is $R_{\rm bin} \approx 419$ μas.

Thus, using for the highest values of the error bars the values $\Delta_{\rm min} = Beam/5$, we found that the final offset is $\Delta W_t \approx +0.410$ mas, and $\Delta N_t \approx +0.090$ mas, and the radius of the BBH system is $R_{\rm bin} \approx 0.419$ mas.

These values have to be compared with the values obtained assuming for the lowest error bars the value used $\Delta_{\rm min} = Beam/15$, which are $\Delta W_t \approx +0.405$ mas, and $\Delta N_t \approx +0.110$ mas, and the radius of the BBH system is $R_{\rm bin} \approx 0.420$ mas.

C.7. Final solution

The characteristics of the final solution determined assuming for the minimum value of the error bars the value $\Delta_{\rm min} = Beam/5$ are

- $T_{\rm p}/T_{\rm b} \approx 140$;
- $M_1/M_2 \approx 2.75$;
- $i_{\rm o} \approx 11.0°$; and
- $\chi^2_{\rm min} \approx 28.9$.

Thus the reduced χ^2 at the minimum is $\chi^2_{\rm r} \approx 0.19$, indicating that the minimum error bars are too large.

C.8. Conclusion

We determined the characteristics of the solution, assuming for the minimum value of the error bars the value $\Delta_{\rm min} = Beam/5$ suggested by Lister & Homan (2005). We found that

1. the characteristics of the solution are the same as those of the solution determined assuming for the minimum value of the error bars the value $\Delta_{\rm min} = Beam/15$, and
2. the corresponding reduced χ^2 is $\chi^2_{\rm r} \approx 28.9/152 \approx 0.19$, indicating that the minimum error bars are too large.

The correct value for the minimum error bars at 15 GHz is $Beam/15 \leq \Delta_{\rm min} \leq Beam/12$.

This value

1. produces a reduced χ^2, $\chi^2_{\rm r} \approx 1$;
2. the minimum value agrees with the value of the realistic error obtained from the VLBI Service for Geodesy and Astrometry (Schlüter & Behrend 2007), and
3. the fit of VLBI coordinates of components of 3C 345 (work in progress) indicates that the adopted values for the minimun values of the error bars, i.e., $Beam/15 \leq \Delta_{\rm min} \leq Beam/12$, are correct for frequencies between 8 GHz and 22 GHz.

References

Achatz, U., & Schlickeiser, R. 1993, A&A, 274, 165
Attridge, J. M., Roberts, D. H., & Wardle, J. F. C. 1999, ApJ, 518, L87
Biretta, J. A., Sparks, W. B., & Macchetto, F. 1999, ApJ, 520, 621
Britzen, S., Roland, J., Laskar, J., et al. 2001, A&A, 374, 784
Burke-Spolaor, S. 2011, MNRAS, 410, 2113
Camenzind, M., & Krockenberger, M. 1992, A&A, 255, 59
Caproni, A., Livio, M., Abraham, Z., & Mosquera Cuesta, H. J. 2006, ApJ, 653, 112
Cohen, M. H., Cannon, W., Purcell, G. H., et al. 1971, ApJ, 170, 207
Cotton, W. D., Counselman, III, C. C., Geller, R. B., et al. 1979, ApJ, 229, L115
Falomo, R., Urry, C. M., Pesce, J. E., et al. 1997, ApJ, 476, 113
Fey, A. L., Gordon, D. G., Jacobs, C. S. 2009, IERS Technical Note No. 35 (Frankfurt: Bundesamts für Kartographie und Geodäsie)
Gabuzda, D. C., & Cawthorne, T. V. 1996, MNRAS, 283, 759
Gabuzda, D. C., Cawthorne, T. V., Roberts, D. H., & Wardle, J. F. C. 1989, ApJ, 347, 701
Gabuzda, D. C., Mullan, C. M., Cawthorne, T. V., Wardle, J. F. C., & Roberts, D. H. 1994, ApJ, 435, 140
Glück, C. B. 2010, in Diplomarbeit, Universität zu Köln
Goldschmidt, P., Kukula, M. J., Miller, L., & Dunlop, J. S. 1999, ApJ, 511, 612
Gómez, J.-L., Marscher, A. P., Alberdi, A., Jorstad, S. G., & Agudo, I. 2001, ApJ, 561, L161
Hébrard, G., Lemoine, M., Vidal-Madjar, A., et al. 2002, ApJS, 140, 103
Jorstad, S. G., Marscher, A. P., Lister, M. L., et al. 2005, AJ, 130, 1418
Katz, J. I. 1997, ApJ, 478, 527
Kellermann, K. I., Sramek, R., Schmidt, M., Shaffer, D. B., & Green, R. 1989, AJ, 98, 1195
Kharb, P., Capetti, A., Axon, D. J., et al. 2012, AJ, 143, 78
Lampton, M., Margon, B., & Bowyer, S. 1976, ApJ, 208, 177

Lawrence, C. R., Pearson, T. J., Readhead, A. C. S., & Unwin, S. C. 1986, AJ, 91, 494
Lister, M. L., & Homan, D. C. 2005, AJ, 130, 1389
Lister, M. L., Tingay, S. J., Murphy, D. W., et al. 2001, ApJ, 554, 948
Lister, M. L., Aller, H. D., Aller, M. F., et al. 2009a, AJ, 137, 3718
Lister, M. L., Cohen, M. H., Homan, D. C., et al. 2009b, AJ, 138, 1874
Lobanov, A. P. 1998, A&A, 330, 79
Lobanov, A. P., & Roland, J. 2005, A&A, 431, 831
Ma, C., Arias, E. F., Eubanks, T. M., et al. 1998, AJ, 116, 516
Marcowith, A., Henri, G., & Pelletier, G. 1995, MNRAS, 277, 681
Marcowith, A., Henri, G., & Renaud, N. 1998, A&A, 331, L57
Marziani, P., Sulentic, J. W., Dultzin-Hacyan, D., Calvani, M., & Moles, M. 1996, ApJS, 104, 37
Miller, L., Peacock, J. A., & Mead, A. R. G. 1990, MNRAS, 244, 207
Muxlow, T. W. B., Pelletier, G., & Roland, J. 1988, A&A, 206, 237
O'Dea, C. P., Barvainis, R., & Challis, P. M. 1988, AJ, 96, 435
Peacock, J. A., Miller, L., & Longair, M. S. 1986, MNRAS, 218, 265
Pearson, T. J., & Readhead, A. C. S. 1988, ApJ, 328, 114
Pelletier, G., & Roland, J. 1989, A&A, 224, 24
Pelletier, G., & Roland, J. 1990, in Parsec-scale radio jets, eds. J. A. Zensus, & T. J. Pearson (Cambridge University Press), 323
Pelletier, G., & Sol, H. 1992, MNRAS, 254, 635
Pelletier, G., Sol, H., & Asseo, E. 1988, Phys. Rev. A, 38, 2552
Roland, J., Britzen, S., Kudryavtseva, N. A., Witzel, A., & Karouzos, M. 2008, A&A, 483, 125
Roland, J., Britzen, S., Witzel, A., & Zensus, J. A. 2009, A&A, 496, 645
Roland, J., & Hermsen, W. 1995, A&A, 297, L9
Roland, J., & Hetem, A. 1996, in Cygnus A – Study of a Radio Galaxy, eds. C. L. Carilli, & D. E. Harris (Cambridge University Press), 126
Roland, J., Pelletier, G., & Muxlow, T. W. B. 1988, A&A, 207, 16
Roland, J., Teyssier, R., & Roos, N. 1994, A&A, 290, 357
Schlüter, W., & Behrend, D. 2007, J. Geodesy, 81, 379
Shepherd, M. C. 1997, in Astronomical Data Analysis Software and Systems VI, eds. G. Hunt, & H. Payne, ASP Conf. Ser., 125, 77
Skibo, J. G., Dermer, C. D., & Schlickeiser, R. 1997, ApJ, 483, 56
Sol, H., Pelletier, G., & Asseo, E. 1989, MNRAS, 237, 411
Tingay, S. J., & Wayth, R. B. 2011, AJ, 141, 174
Tingay, S. J., Jauncey, D. L., Reynolds, J. E., et al. 1998, AJ, 115, 960
Unwin, S. C., Cohen, M. H., Hodges, M. W., Zensus, J. A., & Biretta, J. A. 1989, ApJ, 340, 117
Wehrle, A. E., Piner, B. G., Unwin, S. C., et al. 2001, ApJS, 133, 297
Whitney, A. R., Shapiro, I. I., Rogers, A. E. E., et al. 1971, Science, 173, 225